

https://dspace.org/

CHemical inhibitors in gas hydrate formation A review of modelling Approaches

Njabulo Zulu; Hamed Hashemi; k Tumba

https://hdl.handle.net/10539/43416
SCOPUS

Downloaded from a DSpace repository. https://dspace.org/

ChemEngineering

MDPI

Review

Chemical Inhibitors in Gas Hydrate Formation: A Review of Modelling Approaches

Njabulo Mziwandile Zulu [1,2], Hamed Hashemi [1] and Kaniki Tumba [2,*]

[1] School of Chemical and Metallurgical Engineering, University of the Witwatersrand, 1 Jan Smuts Avenue, Braamfontein, Johannesburg 2001, South Africa
[2] Thermodynamics-Materials-Separations Research Group, Department of Chemical Engineering, Mangosuthu University of Technology, uMlazi, Durban 4031, South Africa
* Correspondence: tumba@mut.ac.za

Abstract: Gas hydrate inhibition using chemicals has been under continuous investigation, and several modelling studies have been published since its inception. Since it is not always feasible to conduct experimental research, it is especially crucial to forecast the conditions under which gas hydrates may form and dissociate in the presence of chemical inhibitors. As a result, a reliable forecasting tool is vital. This article provides an exhaustive review of various modelling methodologies in the context of gas hydrate chemical inhibition. The key aspects of empirical models, thermodynamic models, kinetic models, artificial intelligence-based models and quantum chemistry-based models are presented. Critical analysis of each modelling approach has been performed, highlighting strengths, limitations, and areas where further investigations are still crucial. Rapid progress has been made with respect to gas hydrate modelling approaches in the context of chemical inhibition; however, further research is still vital to bridge the gaps that have been identified in this review. Potential improvements to existing models have been proposed, particularly in terms of integrating experimental data and utilizing hybrid approaches, which could serve as valuable future directions for the field.

Keywords: gas hydrates; chemical inhibition; modelling

Citation: Zulu, N.M.; Hashemi, H.; Tumba, K. Chemical Inhibitors in Gas Hydrate Formation: A Review of Modelling Approaches. *ChemEngineering* **2024**, *8*, 124. https://doi.org/10.3390/chemengineering8060124

Academic Editors: Amadeu K. Sum

Received: 27 August 2024
Revised: 26 September 2024
Accepted: 15 November 2024
Published: 3 December 2024



Copyright: © 2024 by the authors. Licensee MDPI, Basel, Switzerland. This article is an open access article distributed under the terms and conditions of the Creative Commons Attribution (CC BY) license (https://creativecommons.org/licenses/by/4.0/).

1. Introduction

One of the most significant flow assurance issues is gas hydrate formation during natural gas production, processing, and transmission. Gas hydrates can cause blockages in pipelines, which can negatively impact transmission safety and significantly interrupt operations [1]. The necessity of resolving this problem has sparked interest in research on gas hydrate formation mitigation. Numerous researchers have been examining different gas hydrate prevention techniques for a number of years [2,3]. Chemical inhibition is the most frequently employed and efficient means of preventing gas hydrate generation [4,5].

Experimental investigation is not always viable and therefore, appropriate modelling approaches for predicting the impact of chemical inhibitors on hydrates of natural gases should be sought. Multiple investigations have been undertaken over many years, with several chemical inhibition approaches being proposed with some distinct modelling methodologies [6].

A thorough understanding of various accurate modelling tools is necessary to enable flow-assurance workers in the oil and gas industry to make well-informed decisions when mitigating the development of gas hydrates in pipelines using chemicals. Therefore, a comprehensive review of suitable modelling approaches should be available, and this article is intended to provide an in-depth review of different gas hydrate modelling approaches in the context of chemical inhibition. The primary objectives of this research are as follows:

(1) highlight developments in gas hydrate modelling in the context of chemical inhibition.
(2) identify areas of potential further research in modelling gas hydrate systems in the presence of chemical inhibition.

While a review paper previously published on this subject matter concentrated primarily on general gas hydrate modelling techniques [7], this work emphasizes gas hydrates modelling approaches in relation to chemical inhibition. It offers a comparative analysis of different models, highlighting their strengths and limitations in ways that have not been previously explored in detail.

2. Background on Gas Hydrates

2.1. Definition

Gas hydrates are sub-groups of compounds known as clathrate hydrates. These are a special type of inclusion complexes composed of two molecules that organize themselves in space such that the guest molecule is confined within the host [8]. In gas hydrates, the gas molecules are confined inside the cage of water molecules [9]. When the guest molecules engage with the host molecules through Van der Waals intermolecular forces, a cage-like structure, known as clathrate hydrate, is formed [10]. In gas hydrates, there is no interaction between the guest and host molecules; therefore, the former molecules are free to rotate within the framework formed by the latter molecules [9]. Figure 1 illustrates the three crystal forms that the majority of natural gas hydrates typically correspond to: structure I (type-I), structure II (type-II), and structure H (type-H) [11]. Type-I, type-II, and type-H hydrates consist of 46, 136, and 34 water molecules, respectively [12]. A gas hydrate forms when the following requirements are met: the presence of gas molecules and the existence of water molecules at low temperature and high pressure conditions [12].

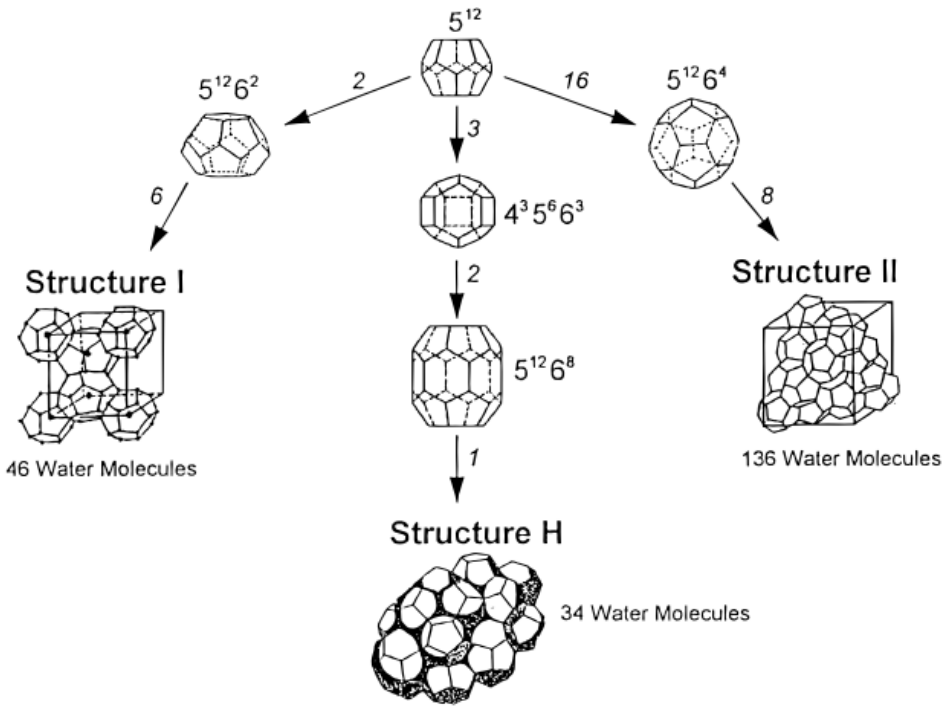


Figure 1. Three common gas hydrate structures (I, II, and H) that are comprised of five distinct water cages [13].

2.2. History of Gas Hydrate Research

Gas hydrates were first recognized by Sir Humphrey Davy in 1810 [13]. It was then experimentally certified by John Faraday in early 1820 [14]. Nonetheless, gas hydrates remained a matter of academic interest until they were identified by Hammerschmidt [1] as being responsible for blockages in oil and gas transmission lines. It was at that time when the industry, government, and academia began an intensive effort to investigate natural gas hydrates [8]. Since then, various researchers have been constantly investigating different gas hydrate prevention measures [2,3,15]. A great deal of study has been conducted in this area regarding the impact of inhibitors on equilibrium conditions [14].

2.3. Properties

The chemical inhibition of gas hydrates requires an understanding of their thermodynamic and kinetic characteristics. The thermodynamic stability of gas hydrates is affected by factors such as temperature, pressure, gas composition, and condensed phase composition (which involves hydrocarbon in the liquid phase, salt content, and the chemical inhibitor) [7]. In thermodynamic gas hydrate inhibition, determining the temperature and pressure conditions at which the flow system would be inside the hydrate stability zone and assessing the settings surrounding gas hydrate dissociation are crucial. Figure 2 depicts the pressure and temperature profile to which a typical fluid can be subjected to inside a flow system. The hydrate formation occurs in the stable hydrate zone. The addition of a thermodynamic inhibitor in the pipeline can cause the hydrate stabilization zone to migrate to lower-temperature and higher-pressure conditions. The kinetics of hydrate growth are a complicated process, in contrast to the thermodynamic characteristics of gas hydrates. Several kinetic factors can impact the nucleation and development of hydrates, and consequently the dissolution of hydrates in water–gas systems [16]. The driving forces, which include temperature and pressure, composition, and interfacial area, are some examples of these factors [11].

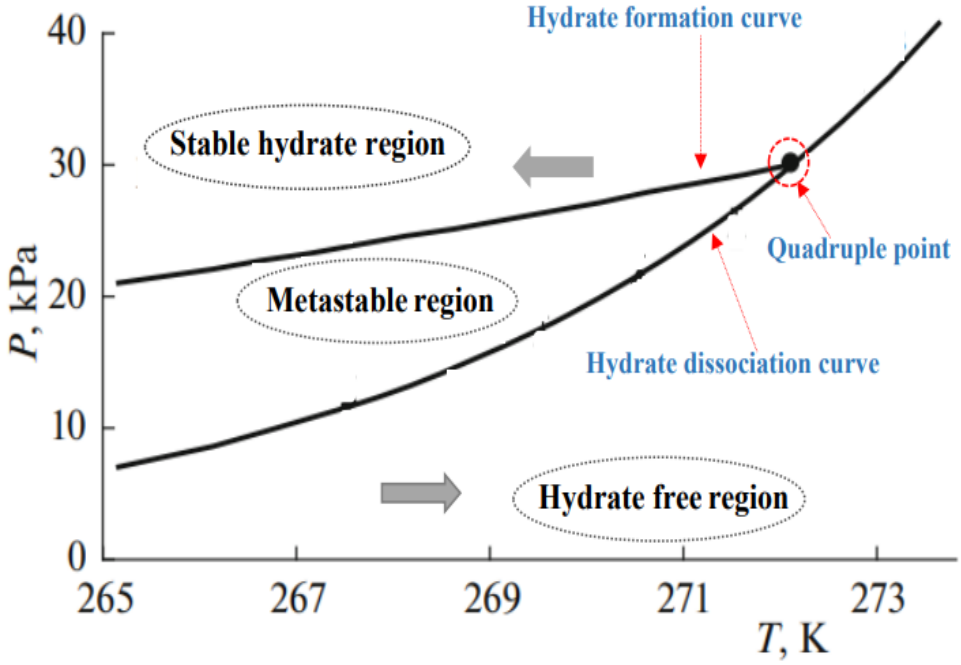


Figure 2. The equilibrium settings and locations of the metastable phases of Freon-12 gas [17].

2.4. Challenges in the Formation of Gas Hydrates

In the oil and gas industry, the accumulation of gas hydrates eventually plugs the gas transmission lines, which leads to uneconomical operation and production stoppages

[8]. The formation of a plug divides the pipeline into two sections: an upstream segment with high pressure and a downstream section with low pressure. As the pressure differential between these two sections rises, the plug may damage the pipe. This may endanger personnel safety and compromise the integrity of the production equipment [18]. During the processing of marine hydrates, external parameters, such as temperature and pressure, may be unpredictably modified, which may lead to hydrate dissociation, enhancing the greenhouse effect via gas emissions. As a result, it is critical to consider safe and environmentally friendly gas hydrate production [19].

The conventional approach for preventing the development of gas hydrates in pipelines is to utilize thermodynamic chemical inhibitors such as methanol and glycol at high concentrations of up to 60 weight percent. Large volumes of methanol and glycol are required, which drives up costs and creates logistical and environmental issues [20].

2.5. Innovative Applications of Gas Hydrates

Despite their negative implications in gas and oil industries, gas hydrates have several beneficial applications. Natural gas hydrate deposits can be used to produce gas, which the global economy needs as an unconventional energy source. More than 230 natural gas hydrate deposits have been found on earth, and this can sufficiently supply energy for many years [21]. Gas hydrates are also useful for the storage and transmission of gas [22]. The process of storing and transporting gas in the form of gas hydrates is more cost-effective than traditional storage techniques such as liquefaction because less infrastructure and equipment are needed. Gas hydrate crystallization is a novel method for separating carbon dioxide from combustion exhaust gas [23]. In addition to carbon dioxide, other greenhouse gases, such as methane, hydrogen sulphide, nitrogen, and others, have also been investigated in relation to gas hydrate separation techniques [22,24]. The water desalination process also includes the application of gas hydrates [8]. The use of gas hydrate formation to concentrate dilute aqueous solutions, including fruit juices, has also been investigated [25]. The utilization of carbon dioxide gas hydrates for separating ionic liquids from dilute aqueous solutions has also been proposed [26].

3. Gas Hydrate Inhibition

3.1. Principle

In the oil and gas sector, hydrates are considered as problematic because they block transmission lines, which poses a safety risk and leads to financial loss [1]. Thus, it is crucial to implement reasonable and safe measures to stop the buildup of gas hydrates in pipelines during the transit of natural gas [4]. As previously stated, the following conditions promote the production of a hydrate: low temperature and high pressure, as well as the presence of water and a gas, such as methane, ethane, or carbon dioxide.

Therefore, gas hydrate inhibition can be performed using at least one of the following four common methods: (1) heating the system above the temperature at which hydrates form; (2) lowering the system pressure to below the hydrate stabilization zone; (3) removing water from the system; (4) introducing specific chemicals to stop or postpone the production of gas hydrate plugs [27]. Chemical inhibition is the commonly used and most effective method for the avoidance of gas hydrate production [4,5].

3.2. Types of Chemical Inhibitors

Chemical inhibitors can be divided into two main groups based on the quantity levels at which they are used, namely high-dosage hydrate inhibitors (HDHI) and low-dosage hydrate inhibitors (LDHI) [5]. High-dosage hydrate inhibitors include thermodynamic hydrate inhibitors (THIs), while low-dosage hydrate inhibitors include kinetic hydrate inhibitors (KHIs) and anti-agglomerates (AAs).

3.2.1. Thermodynamic Hydrate Inhibitors (THIs)

Thermodynamic hydrate inhibitors move the hydrate equilibrium curve towards lower temperature and higher-pressure conditions, maintaining the system out of the hydrate production zone [28]. By breaking the bond of hydrogen that joins water molecules together, a thermodynamic hydrate inhibitor aims to prevent the development of gas hydrates. This hydrogen bond disruption leads the hydrate–liquid–vapor equilibrium curve to shift to a higher pressure and lower temperature. This changes the thermodynamic parameters, encouraging the development of gas hydrates [29]. The most used THIs are electrolytes, methanol, and monoethylene glycols; however, their application is restricted by their high cost and related environmental issues [11]. Consequently, further search for cost-effective and environmentally friendly THIs remains crucial. Furthermore, ionic liquids are regarded as highly attractive THI candidates for effectively dissociating gas hydrates. To stop the formation of cage-like structures, these THIs have the ability to form hydrogen bonds with water molecules. A significant amount of THIs is required to properly disintegrate a gas hydrate in a certain gas stream [30].

3.2.2. Kinetic Hydrate Inhibitors (KHIs)

Low molecular weight polymers in a solvent are the hallmark of kinetic hydrate inhibitors. Unlike THIs that prevent hydrate formation by altering thermodynamic conditions, KHIs postpone the hydrate nucleation period by slowing down the hydrate growth [31]. Compared to traditional THIs such as methanol, KHIs can significantly lower the total cost of hydrate inhibition [32]. The most often utilized KHIs are copolymer derivatives or synthetic polymers that can be either in liquid or solid phase [28].

3.2.3. Anti-Agglomerates (AAs)

Surface-active substances called anti-agglomerates do not prohibit gas hydrates development; instead, they stop pipeline blockages [33]. They keep hydrates from conglomerating, thereby maintaining the fluid viscosity low and allowing the hydrates to be delivered in a slurry state [34]. AAs are more economical and operate better as hydration inhibitors under extremely high pressure compared to KHIs [35]. The mostly used AAs are quaternary ammonium salts and surfactants in the oil and gas sector [28].

3.2.4. Dual Function Gas Hydrate Inhibitors

Compounds known as dual function inhibitors serve as both thermodynamic and kinetic inhibitors by moving the equilibrium hydrate curve to a lower temperature and concurrently lengthening the induction period for gas hydrate development [36]. Ionic liquids have garnered significant attention from researchers due to their potential as dual function hydrate inhibitors [36–38].

3.3. Data Collection Criteria

3.3.1. Review of Equipment

The experimental equipment that is used to measure the phase equilibrium conditions is classified into two main types: dynamic and static techniques [39]. Static techniques are preferred due to their simplicity and applicability at high pressures and various temperatures [40,41]. The major limitation of the static experimental set up is the long time interval that is required before the equilibrium conditions are attained [41]. An alternative experimental set up that may be used to shorten the time required to attain equilibrium is the Quartz Crystal Microbalance (QCM), which uses small amounts of samples [42]. Most of the time, QCM hydrates do not cling to the quartz crystal's surface as they should, and this makes the operation impractical [41]. The objective of the study and the ease with which data are collected influence the choice of experimental equipment used. Among other static apparatus, stirred reactors, autoclaves, crystallizers and high-pressure cells are commonly employed to monitor the temperature, pressure, and agitation strength

when investigating the chemical inhibition of gas hydrates [43]. The autoclave technique is preferred when high shear rates are required; however, the number of tests that can be performed in a particular time span is limited, and this may require a large volume of the sample to be used [44]. Gas hydrate chemical inhibition has also been studied using calorimetric techniques such as differential scanning calorimetry (DSC) [45]. This procedure is relatively quicker than the traditional approaches; however, the inconsistencies in the measured properties using similar calorimetric approaches are significantly higher than the stated experimental uncertainties [41]. Rocking cell equipment has also been used in gas hydrate systems involving chemical inhibition [46]. Although rocking cells typically require a small volume of sample, in water cut investigations which are greater than 60 vol%, the significant volume of hydrates that are generated may result in false negatives due to the restricted mixing taking place in this experimental setup [46].

Titanium and stainless steel are often used to make the cell body. The apparatus typically consists of a magnetic stirrer, a vessel (cell) with a particular capacity that can tolerate high pressures, and a window or cameras to visually monitor the development of gas hydrate. High-precision temperature and pressure probes, as well as gauge/transducers, are necessary for the measurement of the change in these parameters to validate the development of gas hydrates.

The data are recorded using a data acquisition device [47]. Table 1 contains a list of apparatus and a selection of investigators who have utilized them for gas hydrate research in the presence of chemical inhibitors.

Table 1. Apparatus for studying gas hydrates with chemical inhibitors present.

References	Inhibitor	Apparatus	Volume (cm^3)	Pressure (MPa)
[48]	THI	High-pressure cell	500	20
[49]	THI	High-pressure cell	60	20
[50]	THI	High-pressure cell	75	15
[51]	THI	High-pressure cell	650	20
[52]	THI	High-pressure cell	250	20
[53]	THI	Crystallizer	416	30
[54]	THI	Stirred reactor	300	* N/A
[55]	THI	Differential scanning calorimetry	0.5	40
[56]	THI	Hydreval	80	20
[57]	THI	Autoclave	150	* N/A
[58]	KHI	Autoclave	* N/A	* N/A
[59]	KHI	Autoclave	145	40
[60]	KHI	Autoclave	23	* N/A
[61]	KHI	High-pressure cell	90	15
[62]	KHI	High-pressure cell	100	20
[63]	KHI	High-pressure cell	280	10
[15]	KHI	High-pressure cell	300	12
[64]	KHI	Crystallizer	500	20
[65]	KHI	Crystallizer	400	* N/A
[66]	KHI	Stirred reactor	220	* N/A
[67]	KHI	Stirred reactor	300	20
[68]	KHI	Differential scanning calorimetry	0.5–1	40
[69]	KHI	Differential scanning calorimetry	0.5–1	40
[70]	AA	Autoclave	23	* N/A
[70]	AA	Rocking cell	20	* N/A
[71]	AA	Rocking cell	* N/A	20
[72]	AA	Rocking cell	* N/A	* N/A

[36]	THI/KHI	Differential scanning calorimetry	0.5	40
[37]	THI/KHI	Differential scanning calorimetry	0.5	40
[73]	THI/KHI	Differential scanning calorimetry	* N/A	100
[38]	THI/KHI	Stirred reactor	420	20
[74]	THI/KHI	High-pressure cell	150	* N/A
[75]	THI/KHI	High-pressure cell	650	20

* N/A: not applicable or not given in the literature.

3.3.2. Procedure

Three primary procedures (isothermal, isobaric, and isochoric, respectively) were developed for experimental phase equilibrium condition measurements [11,76]. The isothermal approach keeps the system temperature constant, and the equilibrium pressure is established by visually observing the disappearance of the hydrate. In the isobaric approach, the equilibrium temperature is determined by visually observing the hydrate's disappearance while maintaining a constant system pressure. The isochoric approach maintains a constant volume while changing the pressure with temperature and phase change. Since the hydrate dissociation points are found using a pressure vs. temperature plot, the isochoric approach does not require visual observation. The hydrate phase equilibrium conditions are frequently measured using non-visual procedures in most studies [77].

Tohidi et al. [76] demonstrated that for non-visual techniques, the time necessary for dissociation pressure measurement is greatly shortened by increasing the size of the temperature increments. This offers the advantage of enhancing both the testing cost and the dependability of the results. The isochoric pressure search method, which uses the non-visual technique, was implemented for the measurement of the dissociation conditions by [78]. Most researchers have recently used this method in their studies involving measurements of the dissociation conditions [49,51,57,62,79].

3.3.3. Data Presentation and Processing

To examine how chemical inhibitors affect the development of gas hydrates, the hydrate–liquid–vapor equilibrium (HL_wVE) curve is plotted. The plotted curve is then compared to relevant data from published literature to endorse the experimental apparatus and methodology used. The liquid hydrate equilibrium point is obtained from a diagram of pressure against temperature which is drawn for every experimental run. The liquid hydrate equilibrium point is the intersection of the heating and cooling curves as illustrated in Figure 3.

The inhibitory impact of various inhibitors can be determined from the hydrate equilibrium data illustrated in both tabular and graphical presentations. The typical data on hydrate equilibrium for the evaluation of the thermodynamic inhibition effect of methanol (MEG) are summarized in Figure 4 and Table 2. The region where hydrates are thermodynamically in equilibrium is shown on the left side of the curve, and the region devoid of hydrates is shown on the right side [80]. The demonstration of gas hydrate inhibition is represented by the shift of the HLwVE curve to the left of the original curve, into the lower-temperature and higher-pressure zone.

Furthermore, the introduction of a thermodynamic inhibitor transfers the hydrate equilibrium temperature to a lower value at the corresponding pressure, and this results in suppression temperature (ΔT_{eq}). Based on calculated ΔT_{eq} data, the thermodynamic inhibition effect of different inhibitors can be objectively compared at any given concentration and pressure. The greater ΔT_{eq} is, the greater will be the inhibition effect.

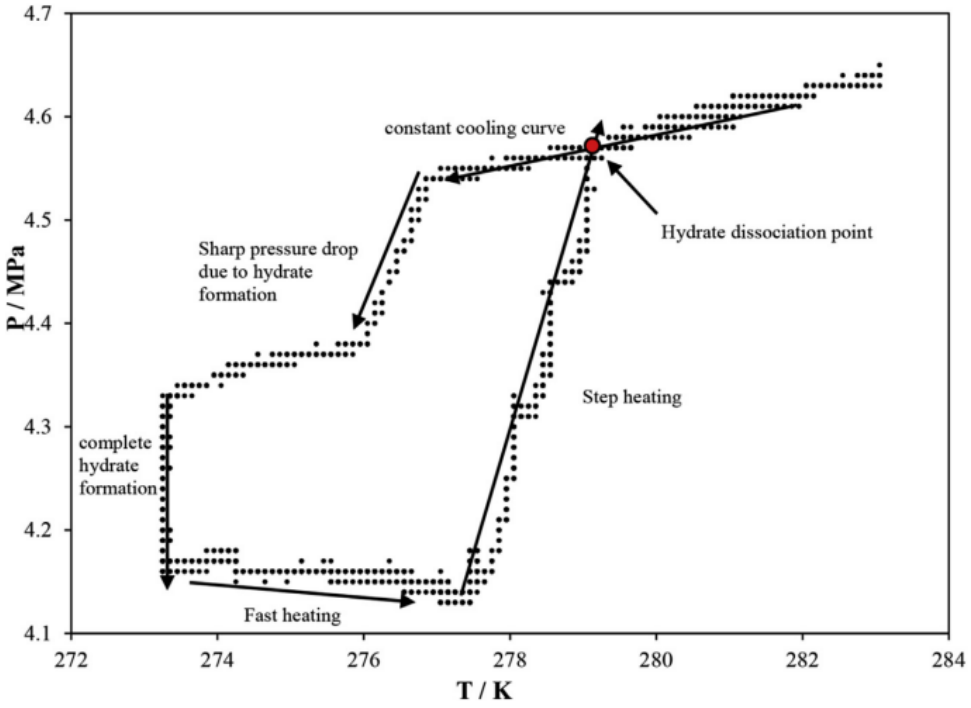


Figure 3. Typical pressure and temperature profile recorded during the experiment with deionized water and methane [81].

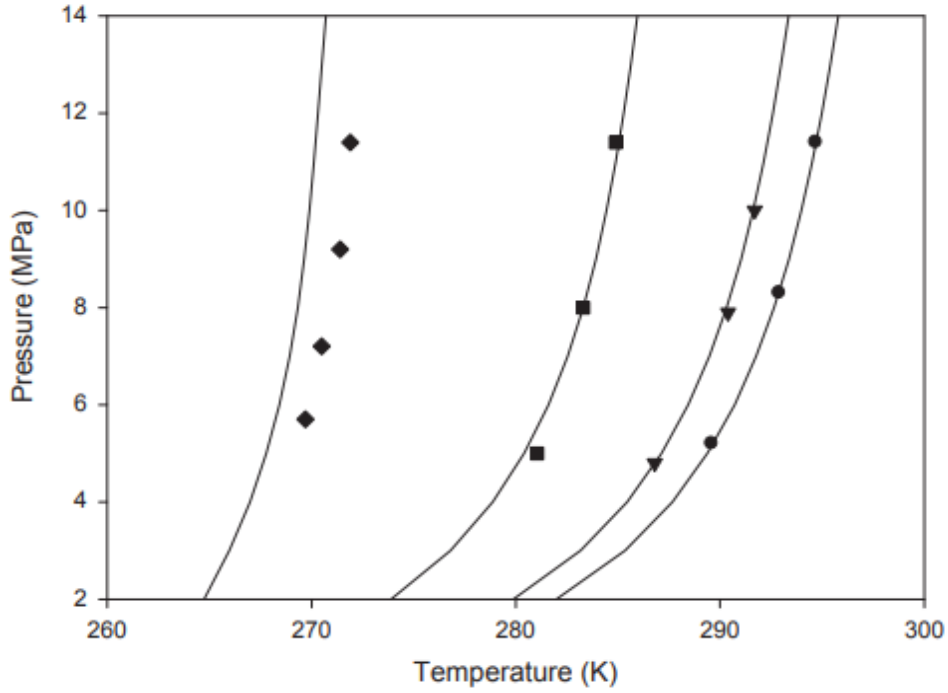


Figure 4. Equilibrium curves of hydrates in pure water (●); 10.0 wt% MEG (▼); 30.0 wt% MEG (■); 50.0 wt% MEG (♦) [80]. Calculated results from CSMGem are indicated by solid lines [11] at corresponding MEG concentrations.

Table 2. Phase equilibrium data for (natural gas + aqueous MEG solutions) at different MEG concentrations [80].

Concentration (wt%)	Pressure (MPa)	Temperature (K)	Calculated ΔT_{eq} (K)
10.0	10.0	291.7	2.3
	7.9	290.4	2.3
	4.8	286.8	2.2
30.0	11.4	284.9	9.6
	8.0	283.3	9.3
	5.0	281.5	8.9
50.0	11.4	271.9	23.7
	9.2	271.4	23.1
	7.2	270.5	22.2
	5.7	269.7	21.3

The typical hydrate equilibrium data used for evaluating the effect of kinetic inhibition effect are summarized in Figure 5 and Table 3. The mechanism of action of kinetic hydrate inhibitors involves postponing the process of hydrate nucleation and development, thereby extending the hydrate onset time. The period between the system entering the hydrate equilibrium region and the first indication of hydrate development is known as the induction or hydrate onset time. Thus, the hydrate onset time indicates how long the development of hydrates is delayed in the presence of kinetic hydrate inhibitors [80]. It should also be noted that the amount of the hydrate former (gas molecules) in the gas phase decreases with the formation of the hydrate. Therefore, the rate at which hydrate is formed may be calculated by monitoring the gas consumption rate. Thus, the kinetic hydrate performance of different inhibitors can be demonstrated in terms of prolonged hydrate induction time and reduced hydrate formation rate. Typically, as shown in Table 3, the hydrate induction time (t_0) is 185.0 min in the presence of the kinetic inhibitor (30.0 wt% MEG solution), which signifies a substantial delay, as compared to 39.0 min in the absence of the inhibitor (pure water). Furthermore, it is clear from observing the gas consumption rates in Figure 5 that, in comparison to pure water, the hydrate development rate for 30.0 wt% MEG solution is extremely low.

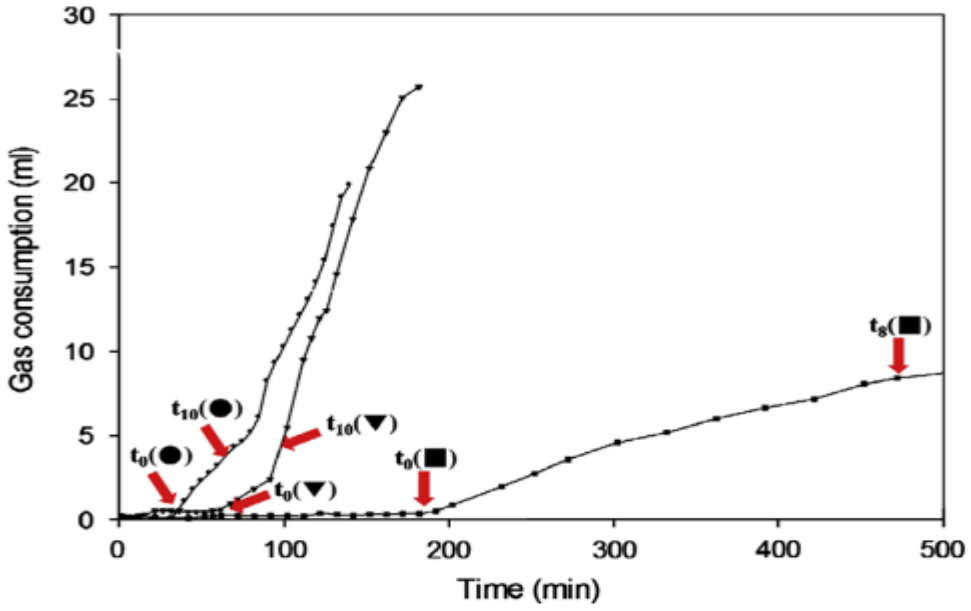


Figure 5. Curves of synthetic gas mixture usage during hydrate formation: pure water (●); 10.0 wt% MEG solution (▼); 30.0 wt% MEG solution (■). The time at which the hydrate equilibrium temperature is reached is known as the time origin [80].

Table 3. Hydrate induction time, subcooling temperature (ΔT_{Sub}) and 10% hydrate conversion time ($t_{10\%}$) in the presence of pure water and 10 and 30 wt% MEG solutions [80].

System	ΔT_{Sub} (K)	t_0 (min)	$t_{10\%}$ (min)
Pure water	7.5	39.0 ± 3.7	79.2 ± 6.5
10.0 wt% MEG	6.8	60.0 ± 6.2	98.0 ± 8.9
30.0 wt% MEG	7.0	185.0 ± 16.5	>354.0

4. Modelling Approaches

4.1. Modelling in the Context of Gas Hydrate Inhibition

In industrial applications, the prediction of gas-hydrate phase equilibrium conditions is very important to successfully inhibit gas hydrate formation. Thus, an accurate modelling approach is required. The first attempt of modelling in the context of gas hydrate inhibition commenced with Hammerschmidt in the 1930s [6]. It was very critical to forecast the effect of inhibitors on the gas-hydrate phase boundary; hence, Hammerschmidt developed a formula that would be used to predict the sufficient quantity of inhibitors required to prevent the possibility of gas hydrate development. The basis of this equation was the reduction in the temperature at which hydrates develop in the presence of inhibitors, and this is a result of the inhibitors' intermolecular interaction with the water molecules. The reduction in equilibrium temperature that is caused by the addition of inhibitors is known as the suppression temperature.

In a search for more accurate prediction tools, the modelling techniques based on thermodynamics were established in the 1950s [6]. The equality of each component's chemical potential throughout all phases is the foundation of thermodynamic models. The presence of the inhibitor changes the phase equilibrium and, as a result, each component's chemical potential in the mixture is also changed. The inhibitor will also cause a considerable alteration in water activity. Therefore, a modelling tool that will accurately predict both the chemical potential and the water activity of each component in the mixture is required. Several thermodynamic models have been proposed and applied to predict the gas-hydrate phase equilibrium in the presence of inhibitors. However, the prediction methods based on the influence of inhibitors on the activity of water were shown to have more accurate results [82].

4.2. Gas Hydrate Inhibition Models

4.2.1. Empirical Modelling

Simple models have been developed to estimate the hydrate inhibition effect of some chemical additives. Most available empirical models have been developed to estimate the magnitude of hydrate equilibrium temperature decrease caused by the addition of inhibitors [83]. As mentioned earlier, the first model that was proposed to determine the temperature at which hydrate suppression occurs when inhibitors are present was the Hammerschmidt equation. This equation is based on the principle which states that the weight of a component dissolved in a specific amount of solvent is directly related to the freezing point lowering, as shown in [84,85].

$$\Delta T_{eq} = \frac{k_H W}{M(100 - W)} \quad (1)$$

where ΔT_{eq} is the suppression temperature in °C, k_H is a constant with a value of 1297, W is the concentration of the inhibitor, expressed as weight percentage in the aqueous phase, and M is the molar mass of the inhibitor, expressed in g/mol. Nevertheless, this equation is restricted to modest doses of typical inhibitors such ethylene glycol and methanol [86]. The Hammerschmidt equation has been modified over time to increase its accuracy by adding parameters based on various types of inhibitors [86]. Nielsen and Bucklin

developed an alternative equation for measuring methanol's hydrate inhibition [87]. Their equation is as follows:

$$\Delta T_{eq} = -72 \ln(1 - x_M) \quad (2)$$

where ΔT_{eq} is the suppression temperature, expressed in °C, and x_M is the mole fraction of methanol. According to Nielsen and Bucklin, the accuracy of this formula is valid up to a mole fraction of 0.8 [86].

The following equation can be used to calculate the weight percent from the mole fraction:

$$X_M = \frac{x_M \, M_M}{18.015 + x_M(M_M - 18.015)} \quad (3)$$

where X_M is the weight fraction methanol, and M_M is the molar mass of methanol.

Despite being designed for use with methanol, the Nielsen–Bucklin equation is independent of the type of inhibitor used [86]. The equation can theoretically be used for any inhibitor because it only considers the concentration of the inhibitor and the characteristics of water.

At low concentrations, the Hammerschmidt and Nielsen–Bucklin equations predict a similar inhibition effect for a given inhibitor solution. Although this Nielsen–Bucklin equation has a wider range of applicability than the Hammerschmidt equation, it has not gained wide acceptance [86]. Most researchers still prefer the simpler Hammerschmidt equation.

Due to constraints on both inhibitor concentration and temperatures in both the Nielsen–Bucklin and Hammerschmidt equations, another modified model for methanol and glycol injection was proposed [88]. The correlations to model the hydrate inhibition effect by methanol and ethylene glycol, respectively, are as follows:

$$\Delta T_{eq} = 0.3938x + 0.006166x^2 \ (Methanol) \quad (4)$$

$$\Delta T_{eq} = 0.1721x + 0.004466x^2 \ (Ethylene\ glycol) \quad (5)$$

where ΔT_{eq} is the suppression temperature in °C and x is the wt% inhibitor in solution. These equations can be generalized to model other inhibitors with appropriate constants.

As brine is the substantial constituent of water that is produced from the oil and gas industry, the estimation of the inhibition impact of salts on gas hydrates is vital. McCain [89] proposed a correlation to forecast how brine will affect the temperature at which hydrates are suppressed.

The following is the correlation:

$$\Delta T_{eq} = AS + BS^2 + CS^3 \quad (6)$$

where ΔT_{eq} is the suppression temperature in °F, S is the salinity in weight percentage, and the coefficients A, B, and C are functions of the gas gravity, γ, and are defined below [86]:

$$A = 2.20919 - 10.5746\gamma + 12.1601\gamma^2 \quad (7)$$

$$B = -0.106056 + 0.722692\gamma - 0.85093\gamma^2 \quad (8)$$

$$C = 0.00347221 - 0.0165564\gamma + 0.049764\gamma^2 \quad (9)$$

The McCain equation is limited to a salt concentration of 20 wt% and for gas-specific gravities in the range of 0.55 to 0.68 [86].

A straightforward correlation to estimate the temperature at which hydrate suppression occurs in systems where the primary hydrate inhibitors are glycerol and salts in

deepwater offshore drilling was developed by Yousif and Young [90]. The following is the correlation:

$$\Delta T_{eq} = 112.3x + 2011.6\,x^2 - 6505.0x^3 \quad (10)$$

where ΔT_{eq} is the suppression temperature in °F, and x signifies the entire mole fraction of the hydrate inhibitors present in the solutions. This correlation predicts the suppression temperature of the hydrate, assuming that the influence of gas composition is insignificant, and hence it is equivalent to the ice suppression temperature [85].

A prediction technique for calculating the hydrate inhibition effects of single and mixed thermodynamic inhibitors was developed by Mohammadi and Tohidi [84] to address the shortcomings in the Yousif and Young equation.

The following is the developed correlation:

$$\Delta T_{eq} = -a\left[\ln(1 - x_{solute}) + b{x^2}_{solute} + \sum(c_{1,i}\,W_i + c_{2,i}{W_i}^2 + c_{3,i}{W_i}^3)\right] \quad (11)$$

where a, b, c_1, c_2, and c_3 are constants, x_{solute} and W_i represent the mole fraction of the organic inhibitor and the weight percentage of salt, i, in the aqueous solutions, respectively. This correlation shows acceptable agreement with experimental data for salts and organic inhibitors at high concentrations [85]. However, it does not consider the impact of pressure on the suppression temperature, which may produce a large disagreement between the experimental data and expected findings, particularly at higher pressures.

Østergaard et al. [91] identified the shortcomings of the Youssif and Young equation and then suggested a modified correlation, taking the effect of pressure into account in a further effort to estimate the hydrate suppression temperature.

$$\Delta T_{eq} = (c_1 W + c_2 W^2 + c_3 W^3)(c_4 \ln(P) + c_5) \times (c_6(P_0 - 1000) + 1) \quad (12)$$

where ΔT is the hydrate suppression temperature in K or °C, W is the concentration of the inhibitor in the liquid water phase expressed in mass%, P is the pressure of the aqueous solution, expressed in kPa, P_0 is the dissociation pressure of pure water at 0 °C, expressed in kPa, and c_1, c_2, c_3, c_4, c_5, and c_6 are parameters related to hydrate inhibitors.

Furthermore, Najibi et al. [92] developed a correlation to estimate the hydrate suppression temperature from the freezing point reduction of aqueous solutions with varying inhibitor concentrations [85].

$$\Delta T_{eq} = 0.6825\Delta T_f \quad (13)$$

where ΔT_{eq} and ΔT_f are the hydrate suppression temperature and freezing point reduction of the aqueous solution, respectively.

To address the limitations of the existing correlations for hydrate suppression temperature, the Hu–Lee–Sum equation was developed. To provide an accurate calculation of the hydrate inhibition impact for various salts, this correlation considers factors such as the effect pressure, hydrate structure, types of hydrates, and the concentration of hydrate inhibitors [85]. The following is the Hu–Lee–Sum equation for the hydrate suppression temperature:

$$\frac{\Delta T_{eq}}{T_0 T} = \beta \times ln a_w = C_1 X + C_2 X^2 + C_3 X^3 \quad (14)$$

where ΔT_{eq} is the hydrate suppression temperature, T_0 and T are the hydrate dissociation temperature with pure water and aqueous solution, respectively. β is a constant which only depends on the hydrate former and type, a_w represents the water activity, X is the effective mole fraction for the salts in solution, and $C_1, C_2,$ and C_3 are fitted coefficients. This correlation is easy and practical for estimating the hydrate suppression temperature at a particular condition in terms of pressure, salt types and concentrations [85].

Although the prediction of hydrate suppression temperature is prevalent among the empirical models, there are some other correlations that estimate the hydrate equilibrium

pressure in the presence of different inhibitor solutions. Bahadori et al. [93] suggested an empirical correlation to estimate the hydrate equilibrium pressures of alkanes when methanol, triethylene glycol, sodium chloride, and ethylene glycol are present.

$$P = a + bT + cT^2 + dT^3 \quad (15)$$

where P (MPa) is the hydrate equilibrium pressure, T (K) is the hydrate equilibrium temperature, and a, b, c, and d are the coefficients of the correlation. The coefficient values are determined by adjusting various parameters based on the quantity of the inhibitor present in the system.

Later, a generalized empirical correlation was proposed to estimate the hydrate formation pressure in the presence of some aqueous saline inhibitor solutions [94].

$$P_{eq} = A_x\left[{T_{eq}}^5\right] + B_x\left[{T_{eq}}^4\right] + C_x\left[{T_{eq}}^3\right] + D_x\left[{T_{eq}}^2\right] + E_x\left[T_{eq}\right] + F_x \quad (16)$$

where P_{eq} (MPa) is the hydrate formation pressure, T_{eq} (K) is hydrate formation temperature, A_x, B_x, C_x, D_x, E_x, and F_x are coefficients of the correlation. The type and amount of salt present in the water determine the values of these coefficients.

The above correlation was further simplified for the accurate prediction of the equilibrium data for other hydrates at high pressure of up to 500 MPa [94].

$$P_{eq} = A_x{T_{eq}}^3 + B_x{T_{eq}}^2 + C_xT_{eq} + D_x \quad (17)$$

where P_{eq} is hydrate formation pressure (MPa), and T_{eq} is the formation temperature of the hydrate. The variables A_x, B_x, C_x, and D_x depend on the type and concentration of salt present in the system. The value of A_x can be determined as follows:

$$A_x = A_4x^4 + A_3x^3 + A_2x^2 + A_1x + A_0 \quad (18)$$

where the variable x is the weight percent of salt in the aqueous phase. Similarly, B_x, C_x, and D_x can be determined as follows:

$$B_x = B_4x^4 + B_3x^3 + B_2x^2 + B_1x + B_0 \quad (19)$$

$$C_x = C_4x^4 + C_3x^3 + C_2x^2 + C_1x + C_0 \quad (20)$$

$$D_x = D_4x^4 + D_3x^3 + D_2x^2 + D_1x + D_0 \quad (21)$$

The parameters $A_0 - A_4$, $B_0 - B_4$, $C_0 - C_4$, and $D_0 - D_4$ and their values vary depending on the quantity of salt in the aqueous phase.

This generalized correlation is strongly recommended for the prediction of hydrate equilibrium data in aqueous saline solutions under low- and high-temperature and pressure conditions [94].

Most of the empirical models are based on experimental data, and they are only applicable for a few types of inhibitors, within a small range of concentration and temperature. The main advantage of empirical models is their small number of input parameters, which enable the quick prediction of the hydrate formation conditions [95]. Although the utilization of empirical models to calculate the phase equilibrium of gas hydrates is convenient and straightforward, their application scope is limited due to their excessive dependence on experimental data [96]. Therefore, extending these models to industrial scale operations may be a challenge due to the unavailability of experimental data representative of industrially relevant conditions [97]. Further work is still required to develop empirical models that are applicable for a wide variety of inhibitors, in an extensive range of concentrations and temperatures.

4.2.2. Thermodynamic Modelling

Various thermodynamic models have been proposed for estimating gas hydrate dissociation conditions in the context of inhibitors. These models consider molecular association bonds which are due to the presence of inhibitors in the aqueous phase. The hydrate formation process can be modelled using the thermodynamic equilibrium principle, which states that the chemical potentials of all the constituents in the three phases included are identical (liquid, hydrate, and vapor) [6]. Reviewing the previous studies, the gas hydrate thermodynamic models are categorized into three main types. These types include the van der Waals and Plaatteeuw (vdW-P) model, the Chen-Guo (C-G) model, and the Klauda–Sandler (K-S) model.

The vdW-P Model

The first thermodynamic model for determining the hydrate phase behavior was proposed by van der Waals and Platteeuw [98]. This model was based upon classical adsorption theory. Though it formed a good basis for performing hydrate calculations, van der Waals and Platteeuw's original model was inaccurate when applied to engineering situations. Using the same model, Saito et al. [99] developed a method for predicting hydrate equilibrium conditions which was later generalized by Parrish and Prausnitz [100] to make it suitable for engineering calculations. This model was subsequently modified by Holder et al. [101], and it has been found to provide accurate estimates of hydrate dissociation conditions [102]. In an attempt to improve on the inadequacy of this strategy, which stems from the initial assumptions, John and Holder [103–105], along with John et al. [106] made appropriate modifications to the model.

In the original work, the model is based on the criterion that at equilibrium the chemical potential of water in the hydrate phase (μ_H) and the chemical potential of water in the water-rich or the ice phase (μ_w) are equal. Using the chemical potential of an empty hydrate cage (μ_β) as the reference state, the condition for equilibrium is given as follows:

$$\mu_\beta - \mu_w = \mu_\beta - \mu_H \tag{22}$$

where $\mu_\beta - \mu_w = \Delta\mu_w$, and $\mu_\beta - \mu_H = \Delta\mu_H$.

To calculate $\Delta\mu_w$, Holder et al. [101] presented the following simple relationship:

$$\frac{\Delta\mu_w\,(T,P)}{RT} = \frac{\Delta\mu_w(T_0,P_0)}{RT_0} - \int_{T_0}^{T}\frac{\Delta h_w}{RT^2}dT + \int_{P_0}^{P}\frac{\Delta V_w}{R\bar{T}}dP - \ln a_w \tag{23}$$

where R is the universal gas constant, T is the absolute temperature, P is the pressure, h is the enthalpy, V is the molar volume, $(a_w = \gamma_w X_w)$ is the activity of water in the aqueous phase, γ_w is the activity coefficient of water, X_w is the mole fraction of water in the water-rich solution, the subscript 0 represents a reference state, and the Δ terms represent the change from a pure water phase (either liquid or ice) to a hydrate phase (either type I or II). The bar over the temperature in the last term indicates that this is an average temperature. The first term on the right is the chemical potential difference between the empty hydrate and pure water at the reference temperature, 0 °C,and zero absolute pressure, and it must be experimentally determined. The temperature dependency at constant (zero) pressure is given by the second term. The pressure is adjusted to the ultimate equilibrium pressure by the third term. The final term adjusts the chemical potential from that of a pure water phase to that of an aqueous solution or water-rich phase.

To calculate $\Delta\mu_H$, the following equilibrium model was presented by van der Waals and Platteeuw [98]:

$$\Delta\mu_H = -RT\sum_{i=1}^{2} v_i \ln\left(1 - \sum \theta_{ij}\right) \tag{24}$$

where R is the gas constant, T is the temperature, v_i is the ratio of i-type cavities present to the number of water molecules present in the hydrate phase, and the sum is taken over all components. The variable θ_{ij} is the fraction of i-type cavities which are occupied by j-type gas molecules. According to this equation, the potential interaction between the water and the guest decreases the chemical potential of the hydrate water. The chemical potential of the hydrate water decreases with an increase in the percentage of occupied cavities [102].

The fractional occupancy (θ_{ij}) follows Langmuir's isotherm:

$$\theta_{ij} = \frac{C_{ij} f_j}{\left(1 + \sum_j C_{ij} f_j\right)} \tag{25}$$

where f_j is the gas phase (and hydrate phase) fugacity of the j-type hydrate-forming species, and C_{ij} is the Langmuir constant. The fugacity f_j is related to the mole fraction, y_j, in the gas phase and the total pressure, P, by the following expression:

$$f_j = \varphi_j y_j P \tag{26}$$

where φ_j is the fugacity coefficient.

The interaction between water molecules in a hydrate cavity and the hydrate former is the basis of the computation of the Langmuir constant. Using the Lennard–Jones–Devonshire cell theory, the Langmuir constant is as shown:

$$C_{ij}(T) = 4\frac{\pi}{kT} \int_0^{R_i - a_j} exp\left[-\frac{W(r)}{kT}\right] r^2 dr \tag{27}$$

where k is the Boltzmann constant, $W(r)$ is the spherically symmetric cell potential function, which depends on the subordinate cell radius, coordination number, and the type of guest–host interaction. T is the absolute temperature, r refers to the radial distance from the center of the pore to the center of the guest molecule, R_i is the radius of the hydrate spherical cavity of type i, and a_j is the hydrate-forming radius core of type j. Parrish and Prausnitz proposed the Kihara theory to estimate the cell potential function, as shown below:

$$W(r) = 2z_i\epsilon_j \left[\frac{\sigma_j^{12}}{R_i^{11} r}\left(\delta^{10} + \frac{a_j}{R_i}\delta^{11}\right) - \frac{\sigma_j^6}{R_i^5}\left(\delta^4 + \frac{a_j}{R_i}\delta^5\right)\right] \tag{28}$$

where ϵ_j is the minimum potential, $\sigma_j + 2\,a_j$ is the collision diameter, z_i is the coordination number of each cavity, and δN is calculated for N equal to 4, 5, 10, and 11.

$$\delta^N = \frac{\left[\left(1 - \frac{r}{R_i} - \frac{a_j}{R_i}\right)^{-N} - \left(1 + \frac{r}{R_i} - \frac{a_j}{R_i}\right)^{-N}\right]}{N} \tag{29}$$

The impact of inhibitor addition can be seen on two parameters, which are water activity and fugacity [6]. Water activity is the first parameter, which is presented in Equation (23). The introduction of any component into the mixture, especially the thermodynamic hydrate inhibitor, dramatically changes the activity of water (a_w). Hence, it is critical to quantify the water activity accurately to estimate the inhibitor's influence on the hydrate equilibrium [7]. A predictive model such as UNIFAC or UNIQUAC, along with the VLE approximation combined with G-excess mixing rules, may accurately determine the water activity in the liquid phase [6].

The fugacity of components is the second parameter, which is presented in Equation (25). When a new substance is added to the mixture, the phase equilibrium changes, as does the fugacity of each component. It is generally accepted that there are very few hydrate particles in the system at equilibrium, and that it primarily comprises two phases: vapor and liquid/solid [6]. Consequently, any VSE or VLE computation using the right mixing rule can produce an accurate estimation of fugacity. Therefore, choosing an

appropriate equation of state and mixing rule is the most important stage in the fugacity calculation process. For more intricate hydrocarbon compounds containing highly polar or electrolyte constituents, state equations such as Peng–Robinson or Soave–Redlich-Kwong with the van der Waals mixing rule can be employed. However, advanced EOSs such as Valderrama–Patel–Teja, Nasrifar–Bolland, CPA, or statistical associating fluid theory (SAFT) with the G-excess mixing rules such as MHV1 or MHV2 can be utilized to predict fugacity more accurately [6]. The fundamental disadvantage of the vdW-P type model is the premise that the properties of the empty hydrate lattice are not related to the kind of occupied guest molecules in cavities, which leads to crystal structure distortion following the occupancy of the cavities by the guest molecules [107].

The C-G Model

The second type thermodynamic model, which is statistical mechanics-based, was proposed by Chen and Guo [108,109]. This model represents a two-step process for hydrate production. The first stage assumes that gas molecules contained in water will form unstable clusters, with several water molecules around each guest molecule [109]. Subsequently, these clusters combine to become basic hydrates, wherein the gas molecules completely fill the basic cavities, while all the linked cavities remain unfilled. Basic hydrates encapsulate the empty voids. This stage is correctly explained by the following chemical reaction:

$$H_2O + \lambda_2 G \rightarrow G_{\lambda_2}.H_2O \tag{30}$$

where *G* denotes the gas species, and λ_2 stands for the number of gas molecules per water molecule in the basic hydrate. In the second stage, tiny gas molecules dissolved in water may flow into the unfilled adsorbed cavities, giving hydrates their non-stoichiometric feature.

This stage will, however, not take place for big molecules, as they cannot fit into the cavities. In such a situation, the final hydrate created is simply the stoichiometric basic hydrate formed during the initial stage. Consequently, the fundamental hydrate is real, not just theoretical.

In contrast to the vdW-P model, which balances the chemical potential of water in the hydrate and the fluid phase, the C-G model considers the equality of fugacity of the hydrate former in the hydrate phase and the fluid phase, as follows [110]:

$$f_i^H = f_i^g = f_i^L \tag{31}$$

where f_i^H, f_i^g, and f_i^L are the fugacities of the hydrate former *i* in the hydrate, gas, and liquid phases, respectively.

$$f_i^H = x_i f_i^{HO}\left(1 - \sum_{j=1}^{c} \theta_k\right)^{\alpha} \tag{32}$$

$$\sum_i x_i = 1 \tag{33}$$

$$\alpha = \frac{\lambda_1}{\lambda_2} \tag{34}$$

where x_i is the mole fraction of the gas component i in the large cavities, θ_k is the fraction of tiny cavities that the gas component occupies, $\lambda_1$and λ_2 represent the number of small voids per water molecule and the number of hydrate formers trapped in the basic hydrate (big voids) per water molecule, respectively.

$$\theta_k = \frac{C_k f_k}{1 + \sum_k C_k f_k} \tag{35}$$

C_k is an acronym for the Langmuir constant, which reflects the interactions between the host and guest molecules, and it is calculated as follows:

$$C_k = X_k \, exp\left(\frac{Y_k}{T - Z_k}\right) \tag{36}$$

where X_k, Y_k, and Z_k are the constants of component k that are determined using the data on gas hydrate equilibrium, and their values can be found in the literature [109].

The symbol ${f_i}^{HO}$ in Equation (32) symbolizes the fugacity of the hydrate former in its equilibrium state with the unfilled pure fundamental hydrate i, which is calculated as follows:

$${f_i}^{HO} = f_{T_i}^0 exp\left(\frac{\beta P}{T}\right) {a_w}^{\frac{-1}{\lambda_2}} \tag{37}$$

$$\beta = \frac{\Delta V}{\lambda_2 R} \tag{38}$$

where β is a constant, and a_w is the water activity which can be computed using a suitable equation. When a thermodynamic hydrate inhibitor is not present, the water activity is equal to unity, but when the inhibitor is present, its value is less than unity.

$$f_{T_i}^0 = exp\left(-\sum_i \frac{A_{ij}\theta_{ij}}{T}\right)\left[A_i' exp\left(\frac{B_i'}{T - C_i'}\right)\right] \tag{39}$$

where A_{ij} is the binary interaction parameter expressing the interaction between the guest molecules in the small voids and in the large voids; A_i', B_i', and C_i' are the constants of component i. Their values can be either optimized or found in the literature [109].

The idea of an empty hydrate lattice is replaced in the C-G model with a basic hydrate, whose characteristics depend on the type of guest molecule [107].

The K-S Model

Klauda and Sandler [111] developed the third type of thermodynamic model that relies on the equivalence of fugacities between the hydrate and water. The equivalent of the fugacity of a hydrate in equilibrium with liquid water or ice is given as follows:

$${f_w}^H(T,P) = {f_w}^L(T,P) \text{ or } {f_w}^\alpha(T,P) \tag{40}$$

The following formula is used to determine the fugacity of water in the hydrate phase:

$${f_w}^H(T,P) = {f_w}^\beta(T,P) exp\left(\frac{-\Delta {\mu_w}^H(T,P}{RT}\right) \tag{41}$$

where ${f_w}^\beta(T,P)$ is the fugacity of the theoretical unoccupied hydrate lattice, and $\Delta {\mu_w}^H(T,P)$ is the distinction between the water's chemical potential in the filled hydrate phase and the hypothetical unfilled hydrate lattice, which is expressed as follows:

$$\Delta {\mu_w}^H(T,P) = -RT \sum_m v_m \, ln\left(1 - \sum_j \theta_{mj}\right) \tag{42}$$

where v_m is the number of m-type cages per water molecule in the hydrate structure. The fraction of guest cages that are occupied (θ_{mj}) and the Langmuir constant (C_{mj}) are calculated using Equations (25) and (27), respectively. The cell potential function $W(r)$ includes contributions from the first, second, and third shells:

$$W(r) = W(r)^{[1]} + W(r)^{[2]} + W(r)^{[3]} \quad (43)$$

where $W(r)^{[1]}, W(r)^{[2]}$, and $W(r)^{[3]}$ are the cell potential contributions of the first, second, and third shells of water molecules, respectively. The first shell radii and coordination numbers may be obtained from crystallography measurements [112]. For the second and third shells, the parameters obtained by John et al. [106] may be used.

The Kihara parameters selected for the calculation of the gas–water interaction in the hydrate phase are determined from the following standard mixing rules:

$$\sigma = \frac{\sigma_g + \sigma_w}{2};\ \ \epsilon = \left(\epsilon_g \epsilon_w\right)^{\frac{1}{2}};\ \ a = \frac{a_g + a_w}{2} \quad (44)$$

where σ is the distance between the molecular nuclei when the potential energy is zero, ϵ is the energy parameter, and a is the radius of the molecular core. The subscripts g and w represent the guest in the cavity and the water, respectively.

The fugacity of water in the empty hydrate lattice is calculated as follows:

$$f_w{}^{\beta}(T,P) = P_w{}^{sat,\beta}(T)\emptyset_w{}^{sat,\beta}(T)exp\left(\frac{V_w{}^{\beta}(T,P)(P - P_w{}^{sat,\beta}(T))}{RT}\right) \quad (45)$$

The fugacity of water in ice is determined as follows:

$$f_w{}^{\alpha}(T,P) = P_w{}^{sat,\alpha}(T)\emptyset_w{}^{sat,\alpha}(T)exp\left(\frac{V_w{}^{\alpha}(T,P)(P - P_w{}^{sat,\alpha}(T))}{RT}\right) \quad (46)$$

The fugacity of water in the liquid phase is computed as follows:

$$f_w{}^{L}(T,P) = x_w(T,P)\gamma_w(x_w,T)\ P_w{}^{sat,L}(T)\emptyset_w{}^{sat,L}(T)\ \times exp\left(\frac{V_w{}^{L}(T,P)(P - P_w{}^{sat,L}(T))}{RT}\right) \quad (47)$$

where $P_w{}^{sat,i}(T)$ is the vapor pressure of water in phase i. The fugacity coefficient, $\emptyset_w{}^{sat,i}(T)$, is taken to be unity because the vapor pressures of the water phases are low.

Because of the relatively low solubility of hydrocarbons in liquid water, the solubility is described using Henry's Law [111]. The modified UNIFAC model, as described by Larsen et al. [113], is used to determine each guest molecule's aqueous phase activity coefficient.

The freezing point of water is slightly lower for compounds with a high solubility of guest species in water. By utilizing the following equation, one can estimate the extent of the freezing point depression:

$$\Delta_d T = T_d - T_{nfp} = \frac{R(T_{nfp})^2}{\Delta H_m} ln[x_w \gamma_w(x_w,T)] \quad (48)$$

where T_d is the freezing point with the solute(s) present, T_{nfp} is the normal freezing point of pure water, and ΔH_m is the heat of melting pure ice. The activity coefficient, γ_w, is computed by the modified UNIFAC model.

The C-G model and the K-S model have been shown to provide more precise forecasts regarding the conditions of hydrate formation, as compared to the vdW-P-type models [107].

The significant advantages of thermodynamic models are high accuracy and wide applicable temperature range [96]. Notwithstanding the aforementioned advantages of these models, their main drawback is their complexity in terms of programming and application [114]. Their use as a function of the equation of state is time-demanding because the computation of the inter-molecular interaction and the application of correct mixing rules is conducted through a trial-and-error process [95]. Although several thermodynamic models have been developed to date, further research is still necessary for creating models that are highly accurate over a wide range of conditions that are relevant to the industrial environment. Table 4 presents a review of some previous studies that used the

afore-mentioned types of thermodynamic models for modelling the gas hydrate equilibrium conditions in the presence of various chemical inhibitors.

Table 4. Summary of gas hydrate studies using various thermodynamic models in the presence of chemical inhibitors.

Guest Component	Inhibitor	Model Type	Temperature (K)	Pressure (MPa)	References
CH_4	NaCl	vdW-P	270.66–299.06	6.60–71.56	[115]
C_1–C_3, CO_2	Methanol, glycerol, ethylene glycol, and triethylene glycol	vdW-P	233.1–293	0.18–39.87	[116]
CH_4 CH_4 and CO_2	Tributylmethylphosphonium methylsulfate ionic liquid	vdW-P	273.3–288.5	4.35–14.77	[49]
Pure and mixtures of C_1–C_4	Aqueous imidazolium ionic liquid solutions	vdW-P	298.15–333.5	10–24	[117]
C_1–C_4, CO_2, H_2S	Methanol, Ethanol, MEG, DEG, and TEG	vdW-P	260–300	2.56–71.56	[118]
C_1–C_4, CO_2, H_2S	Methanol, ethanol, glycerol, NaCl, KCl, $CaCl_2$, and $MgCl_2$	vdW-P	239.4–315.1	0.093–328.8	[119]
C_1–C_3	Methanol	C-G	263.34–286.40	0.35–20.4	[120]
C_1–C_4, CO_2, H_2S and N_2	Methanol	C-G	260.3–291.8	0.068–10.79	[121]
C_1–C_3, CO_2 and H_2S	Organic Inhibitors, salts and their mixtures	C-G	260.3–295.1	0.011–39.87	[122]
CH_4	Imidazolium based ionic liquids	C-G	272–287	2.5–11.9	[123]
CH_4	Organic Inhibitors	C-G	234.5–296.75	2.38–50.41	[124]
C_1–C_3, CO_2	Porous media and NaCl or Methanol	C-G	267.28–287.67	0.199–383	[125]
CH_4	Ionic liquids	K-S	273.6–291.59	1.01–20.77	[126]
C_1–C_2, CO_2	NaCl	K-S	261.8–299.1	0.54–71.56	[127]
CH_4	NaOH, $Ca(OH)_2$	K-S	276.60–283.22	4.27–7.90	[128]
CH_4, C_3H_8, H_2S	Methanol, NaCl, $CaCl_2$	K-S	276.75–290.25	0.36–12.87	[129]
CH_4	NaCl	vdW-P	270.66–299.06	6.60–71.56	[115]

4.2.3. Kinetic Modelling

The hydrate formation process is subdivided into nucleation and growth phases. The nucleation process is the formation of stable critical-sized hydrate nuclei, while the growth process is the development of these stable nuclei into solid hydrates [130]. The multicomponent system (water, gas, and hydrate), distributed across multiphases (aqueous, gas, and hydrate) at a multiscale level (macroscopic and molecular), is a feature of the hydrate growth process [131]. At the macroscopic-scale level, the rate of gas hydrates growth can be quantified based on the gas consumption rate, calculated using pressure (P) and temperature (T) [132], as well as direct visualization techniques, such as those measuring hydrate film thickness and morphology [133]. At the molecular-scale level, hydrates growth can be computed based on three controlling mechanisms, namely (i) heat transfer, (ii) intrinsic kinetics, (iii) mass transfer, or a combination of the three. The transfer of gas molecules (guests) from one phase to another should be taken into account in the rate equation, since hydrate formation is typically thought of as an interfacial phenomenon [134].

Kinetic hydrate inhibitors delay the hydrate nucleation and growth rates by increasing the induction time, which is commonly known as the time taken for the formation of stable hydrate nuclei. Therefore, it is necessary and vital to develop kinetic models that may accurately predict delayed hydrate formation rates or increased hydrate induction times, in order to assess the performance of different KHIs. A significant quantity of research has been reported on hydrate formation kinetic models since the 1980s. However, this review will concentrate on models that have been applied in hydrate kinetic inhibition. A generic hydrate nucleation model was developed by Kvamme et al. [135] using the phase field theory to explain how carbon dioxide hydrates nucleate in aqueous solutions. However, low accuracy in terms of hydrate kinetic predictions has been reported due to

the stochastic character of hydrate nucleation and its reliance on equipment and other variables [6]. An intrinsic hydrate growth kinetic model was developed by Englezos et al. [136] to describe the data for the development of methane and ethane hydrates by integrating crystallization and mass transport theories at a gas–liquid interface. The suggested model states that hydrate production consists of three steps [137]:

1. The guest molecule diffuses from the gas–liquid interface to the liquid bulk.
2. The guest molecule's migration from the liquid bulk to the hydrate–solution interface.
3. The water and guest molecules react at the interface between the hydrate and the solution.

The difference between the fugacity of the dissolved gas at the operating temperature and pressure (f) and the three-phase equilibrium fugacity at the operating temperature (f_{eq}) is the driving force for hydrate development.

The rate at which the hydrate grows is expressed as follows:

$$\left(\frac{dn}{dt}\right)_p = K^* A_p (f - f_{eq}) \tag{49}$$

where n represents the moles of gas consumed during hydrate formation, A_p is an interfacial area of a hydrate particle, and K^* is the kinetic constant. This model was applied by Dholabhai et al. [138] to determine the rate at which methane hydrate forms in aqueous electrolyte solutions and to confirm that it closely agrees with the experimental results. The model was slightly adjusted by Malegaonkar et al. [139] for application to more soluble gases, such as carbon dioxide. It is imperative to draw attention to a few applicability limitations of the Englezos–Bishnoi fugacity model [131]:

(i) Fitting experimental data yielded kinetic rate constants for sI-type gas hydrates, exclusively. Because of this, the model can only be used for sI-type gas hydrates, and it is still necessary to quantify the kinetic rate constants for sII- and sH-type gas hydrates.
(ii) The kinetic rate constants were obtained in a laboratory setting using a stirred reactor with an ideal stirring speed, causing issues in estimating the liquid–gas interface area and the hydrate particle surface area.
(iii) The model may not be appropriate for real-time systems because it was created based on apparatus-dependent experimental data [6].

Based on the critical review of Englezos et al.'s [136] model, Skovborg and Rasmussen [140] proposed a modified model, eliminating the population balance equation and considering that all resistance to mass transfer during hydrate formation originates from the movement of the dissolved gas from the gas–liquid interface to the liquid bulk. Consequently, the rate of gas consumption is determined by

$$\frac{dn}{dt} = k_L A_{GL} C_w^0 (x_{int} - x_b) \tag{50}$$

where k_L is the mass-transfer coefficient at the gas–liquid interface, fitted with the aid of experimental data, A_{GL} is the total interfacial area in the reactor, C_w^0 is the initial molar concentration of water, x_{int} is the gas mole fraction in the liquid, in equilibrium with the gas at the interface, and x_b is the gas mole fraction in the liquid bulk, in equilibrium with the hydrate phase, under the operating conditions of the reactor.

Extending Equation (50) to multicomponent gas mixtures containing NG hydrate-forming species, the gas consumption rate is expressed as follows:

$$\frac{dn_T}{dt} = \sum_{i=1}^{NG} \left(\frac{dn_i}{dt}\right) = C_w^0 \sum_{i=1}^{NG} k_{L,i}\, a_{GL} (x_{int,i} - x_{b,i}) \tag{51}$$

where i represents the component i in the gas phase, NG is the number of hydrate-forming compounds in the gas mixture, and a_{GL} is the interfacial area by unit volume.

Herri et al. [141] proposed a new kinetic model to predict the kinetics of methane hydrate formation at constant pressure in a gas–liquid reactor. The reactor is separated into two discrete sections based on the suggested model [137]:

(a) A thin interfacial area where the initial nucleation occurs because of high supersaturation.
(b) The liquid bulk where crystal development and initial nucleation take place, depending upon supersaturation.

The consumption rate is expressed as follows:

$$\frac{dC_b}{dt} = k_L A_{GL}(C_{int} - C_b) - \frac{4\pi I \mu_2}{v_H(1 - x_H)} \quad (52)$$

where C_b is the concentration of the dissolved gas in the liquid bulk, C_{int} is the concentration of the gas in the liquid in equilibrium with the gas at the interface, I is the crystal growth rate, μ_2 is the second moment of the particle size distribution, v_H is the molar volume of the formed hydrate, and x_H is the volumetric fraction of hydrate in the two-phase solution–hydrate mixture. This model also considers the population symmetry of hydrate crystals.

Christiansen et al. [142] demonstrated that the Gibbs free energy change for hydrate formation is a good estimate of the driving force for hydrate growth. Hydrate growth rates per unit area correlate with the driving force. Driving force calculations suggest that hydrate structures other than the thermodynamically favored structures may form.

Natarajan et al. [143] developed a simple model to predict the induction time, based on crystallization theory. They considered the difference in fugacity $\left(f_g^v - f_{eq}\right)$ as the driving force for the gas hydrate development. Crystallization studies suggest that the nucleation rate, R, can be stated as follows:

$$R = k(S - 1)^n \quad (53)$$

where S is the supersaturation ratio, while k and n are constants. Replacing S in Equation (53) by the fugacity ratio, $\frac{f_g^v}{f_{eq}}$, the following expression is obtained:

$$R = k\left(\frac{f_g^v}{f_{eq}} - 1\right)^n \quad (54)$$

Since the induction time is inversely proportional to the nucleation rate, the expression for the induction time is as follows:

$$t_{ind} = \frac{\alpha}{R^r} \quad (55)$$

where α is a proportionality constant, and t_{ind} is the induction time. Since in general the dependence of induction time on the nucleation rate could be non-linear, r could be different than unity. By combining Equations (54) and (55), the following equation is obtained:

$$t_{ind} = K\left(\frac{f_g^v}{f_{eq}} - 1\right)^{-m} \quad (56)$$

where K and m are experimentally adjusted parameters.

To build up the model for the system with kinetic hydrate inhibitors, the following procedure is proposed [144]:

(i) Gas is dissolved in water.
(ii) Gas hydrate nuclei start to grow under stable gas hydrate conditions.
(iii) Kinetic hydrate inhibitors are adsorbed on the surface of the gas hydrate nuclei and reduce the growing rate by decreasing the interfacial area of nuclei.
(iv) The induction time of gas hydrate is increased.

The growth rate of hydrate nuclei with the kinetic hydrate inhibitor is proportional to the active surface area that is free from the inhibitor. The induction time is inversely proportional to this active surface area. If θ is the fractional occupancy covered by kinetic hydrate inhibitors, the fraction of the active surface area is $(1-\theta)$, and the induction time is expressed as follows:

$$t_{ind} = \frac{1}{(1-\theta)} K \left(\frac{f_g^v}{f_{eq}} - 1 \right)^{-m} \tag{57}$$

Kashchiev and Firoozabadi [145] presented the expressions for the supersaturation dependence of the hydrate crystalline growth rate and the induction time in hydrate crystallization. These expressions reveal how the additives in the solution, which act as kinetic inhibitors of hydrate formation, can affect the induction time of the process. The following equation was presented for the prediction of simple gas hydrate formation induction time.

$$t_{ind} = K[S(S-1)^{3m}]^{\frac{1}{(1+3m)}} \times exp\left[\frac{B}{(1+3m)ln^2 S}\right] \tag{58}$$

where t_i is the induction time, K is the kinetic parameter, S is the supersaturation ratio, m is a value greater than zero that results from the crystal growth kinetics, and B is thermodynamic parameter.

Considering the inhibiting effect of some additives in the solution, the following equation was presented for the induction time:

$$t_{ind,a} = K\left[\left(1+k_g C_a\right)^{3m}(1+k_n C_a)\right]^{\frac{1}{(1+3m)}} \times [S(S-1)^{3m}]^{-\frac{1}{(1+3m)}} \times exp\left[\frac{B}{(1+3m)ln^2 S}\right] \tag{59}$$

where $t_{ind,a}$ is the induction time for the additive-containing solution, k_g is the growth site adsorption constant, k_n is the nucleation site adsorption constant, and C_a is the concentration of additive in the solution.

Talaghat and Jokar [146] modified the model of Natarajan et al. [143] to determine the induction time of gas hydrate development in a flow loop system as follows:

$$t_{ind} = K\left(\frac{f_g^v}{f_{eq}} \sqrt{\frac{Q}{Q_0}} - 1 \right)^{-m} \tag{60}$$

where Q is the liquid volumetric flowrate, and Q_0 is a reference volumetric flowrate. The $\frac{Q}{Q_0}$ shows the influence of agitation in a flow system.

Rasoolzadeh et al. [61] developed a chemical kinetics-based model for the induction time of methane hydrate formation in a system where ionic liquids are present. This model's parameters were optimized using a variety of experimental data for a system containing ionic liquids. Natarajan [147] stated that the relation between the induction time (t_{ind}) and the nucleation rate (B^o) is as follows:

$$t_{ind} = \frac{\delta}{(B^o)^{r'}} \tag{61}$$

where r' and δ are constants.

The nucleation rate, B^o, is given by the following equation:

$$B^o = k \exp\left(-\frac{b}{s}\right)^n \tag{62}$$

where k, b and n are arbitrary optimized constants, while s is the supersaturation ratio.

Combining Equations (61) and (62):

$$t_{ind} = \frac{\delta}{k^{r'}} \times \frac{1}{exp\left(-\frac{b}{s}\right)^{nr'}} \tag{63}$$

Replacing $\frac{\delta}{k^{r'}}$ by λ and nr' by m, then Equation (63) becomes:

$$t_{ind} = \lambda\, exp\left(-\frac{b}{s}\right)^{-m} \tag{64}$$

Subcooling is defined as the driving force of supersaturation; therefore, the supersaturation ratio, $s = -\frac{\Delta T}{T_s}$. Then, the induction time equation becomes

$$t_{ind} = \lambda\, exp\left(\frac{bT_s}{\Delta T}\right)^{-m} \tag{65}$$

where λ, m and b are constants which are obtained by the regression of the experimental data, while T_s and ΔT are the supersaturation temperature and subcooling, respectively.

In addition, the inhibition effects of KHIs can be quantitatively described by the chemical affinity model [148]. The chemical affinity model described by Roosta et al. [149] is one of the thermodynamic-based approaches that can be applied for hydrate formation kinetics. The chemical affinity approach has been used for the description of chemical reactions in isothermal–isochoric systems. Therefore, it is applicable to complex systems, such as gas hydrate systems with inhibitors in aqueous solutions [150]. The modelling of the hydrate development rate in a constant volume process makes use of the chemical affinity property [151]. This model defines a macroscopic driving force that just needs temperature and pressure to establish chemical affinity; thus, it does not have the limitations of microscopic models, such as heat and mass transfer coefficients, which are difficult to quantify. To obtain the kinetic parameters of this model (t_k and $-\frac{A_r}{RT}$), the following equation, which was derived by Roosta et al. [149], is used:

$$\frac{A_i}{RT} = -\frac{A_r}{RT}\left[-\ln\left(\frac{t_i}{t_k}\exp\left(1-\frac{t_i}{t_k}\right)\right)\right] \tag{66}$$

where A_i is the chemical affinity at state i, R is the universal gas constant, T is the temperature, A_r is the proportionality constant, which denotes the affinity rate constant, t_i is the time required to reach state i, and t_k is the time required to reach equilibrium conditions.

To predict gas consumption, the following expression is used:

$$\frac{A_i}{Rt} = -ln\frac{n_{ci}}{n_{cf}} \tag{67}$$

where n_{ci} are the moles of gas consumed up to time t_i, and n_{cf} are the total moles of consumed gas.

Combining Equations (66) and (67), the following equation results:

$$\frac{n_{ci}}{n_{cf}} = \left[\left(\frac{t_i}{t_k}\exp\left(1-\frac{t_i}{t_k}\right)\right)\right]^{-\frac{A_r}{RT}} \tag{68}$$

The various kinetic models that have been developed form the basis for replicating the experimental data and anticipating the hydrate growth rate within a comfortable margin [131]. However, most models presented herein are based on fitted parameters that depend on the design of the experimental setup, thus limiting their applicability. It is worth noting that these models do not cover all the significant aspects of kinetic gas hydrate growth, especially in terms of industrial application. Thus, further research is still required to develop a unified model that can be accurately applicable on an industrial scale [6]. Table 5 presents a review of some previous studies that used the kinetic models for modelling gas hydrate formation kinetics in the presence of various kinetic hydrate inhibitors.

Table 5. Summary of gas hydrate studies using various kinetic models in the presence of kinetic hydrate inhibitors.

Guest Component	Inhibitor	Model Type	Temperature (K)	Pressure (MPa)	References
		Hydrate growth rate:			
CH_4	Aqueous electrolyte solutions	Englezos et al.	270–274	3.78–7.08	[138]
Refrigerants	SDS	Englezos et al.	279.9–284.8	0.64–1.1	[152]
C_2H_2, C_2H_4, C_3H_8, and C_3H_6	SDS	Englezos et al.	273.7–280	0.5–4.12	[153]
		Induction time:			
C_1, C_3, CO_2, *i*-C_4	PVP and L-tyrosine	Kashchiev and Firoozabadi model	275–280	1.0–8.0	[154]
Natural gas	Poly vinylpyrrolidone, PVCap, and L-tyrosine	Kashchiev and Firoozabadi model	275–280	1.0–7.0	[155]
Natural gas	Polymeric KHI	Natarajan model	274.15–284.15	5.0	[144]
CH_4	Ionic liquids	Rasoulzadeh and Javanmardi model	272.65–298.15	5.0–6.0	[61]
Natural gas	Methanol, PVP, and L-tyrosine aqueous solution	Rasoulzadeh and Javanmardi model	277.15–293.97	6.0–8.0	[156]
CH_4 and H_2S	PVP and L-tyrosine	Natarajan model	274.15–280.15	10.0	[157]
		Chemical affinity:			
R22	SDS surfactant	Chemical affinity	276.15–285.15	0.35	[158]
THF	Amino acids	Chemical affinity			[159]
C_2H_6	Amino acids	Chemical affinity			[160]
CO_2	Amino acids	Chemical affinity	275.15–285.15	1.58–3.0	[148]
CO_2	Glucose, Attapulgite	Chemical affinity	277.15	3.5	[161]

4.2.4. Artificial Intelligence-Based Modelling

The growing attention on using artificial intelligence techniques for solutions to scientific issues has improved the modelling of the gas hydrate formation behavior in several applications [162]. The most widely employed subset of artificial intelligence (AI) in gas hydrate operations is machine learning (ML) [162]. This method has been actively utilized to model gas hydrate equilibrium, allowing for the development of more accurate models. which can predict the nonlinear and multimodal phenomena of gas hydrate equilibria [163]. ML is a domain of AI that involves training algorithms to make predictions based on available data. Artificial neural network (ANN) models are the most often utilized machine learning models for modelling related to gas hydrates [162]. For the purpose of predicting the conditions of hydrate development for a variety of pure gases, gas mixtures, and inhibitors, an artificial neural network model was developed [164]. A total of 2387 input–output patterns collected from many reliable sources were used to train the model. The predictions were contrasted with real experimental results and with previously established relationships. Without the need for costly experiments, the ANN model provides an accurate forecast of the conditions for hydrate formation for a given gas combination. Gas hydrate modelling has also made use of the group method of the data handling (GMDH) neural network in addition to ANN [165]. The GMDH is the same as ANN; however, it uses quadratic polynomials to model nonlinear patterns between data outputs and inputs. The advantages of GMDH include its ability to forecast and simulate intricate system parameters [162]. It has typically been demonstrated that ANN-based models produce highly precise predictions [166]; nevertheless, one of their drawbacks is that the results are not reproducible, which could be partly attributed to the random initialization of the networks and variation in the stopping criteria during optimization [167]. To address these limitations, Vapnik [168] developed the support vector machine (SVM). The SVM is a tool composed of a collection of connected supervised learning techniques that examine

data and identify trends for regression analysis [169]. As opposed to ANN, the advantages of SVM in hydrate modelling stem from its capacity to handle overfitting [162].

The SVM model was modified by Suykens and Vandewalle [170] to make the initial SVM algorithm set of nonlinear equations easier to solve. The improved version is called the least square support vector machine model (LSSVM). Compared to the SVM, the LSSVM has a better convergence rate and is capable of modelling complex processes using vast amounts of data [162].

Another model that makes use of the mathematical theory of conventional fuzzy sets is fuzzy logic (FL) [171]. Membership functions (MFs) are used in fuzzy logic to transition between real-world and fuzzy models [172]. Gas hydrate modelling in several settings has been performed using FL. The use of FL in nonlinear complex arbitrary functions may yield accurate modelling results [162]. The Takagi–Sugeno fuzzy model was proposed by Takagi and Sugeno [173] as a linear system mathematical tool that expresses the local dynamics of each fuzzy implication.

The adaptive neuro-fuzzy inference system (ANFIS), which combines ANN and the Takagi–Sugeno-type fuzzy systems, is widely utilized for hydrate formation behavior modelling [174]. In complex nonlinear systems, the ANFIS model has demonstrated strong prediction performance [174]. This advantage also promotes its use in studies involving gas hydrates [162].

Another machine learning model frequently employed in gas hydrate research is the Random Forest (RF) [162]. Each tree in the decision trees yields estimates from the RF algorithm [175]. The straightforwardness of parallel implementation, quick training, and forecasting are the foundations of its advantages. Another machine learning model that has been employed in gas hydrate systems is the k-nearest neighbors (KNN). Applications of RF and KNN in gas hydrate environments are well-established, with promising efficiency [162].

The nonlinear autoregressive models with exogenous inputs (NARX) have also been used to predict the gas-hydrate phase behavior [162]. The utilization of NARX in gas hydrate research is encouraged by its capacity to handle nonlinear data and patterns [176]. Gas hydrate modelling has also made use of deep neural network (DNN) approaches, such as feedforward neural networks [162]. It has also been demonstrated that the extra trees method and the hybrid artificial neural network (HFGA) are effective methods for estimating the hydrate dissociation pressure both in the presence and absence of inhibitors [162].

Machine learning has mainly been employed in most investigations to forecast equilibrium data related to hydrate phase behavior. The hydrate inhibitory effect in a variety of systems, including alcohol, salts, and ionic liquids, is the primary focus of these investigations. However, only few research studies have employed machine learning to forecast the hydrate formation kinetics [162]. These models have higher prediction accuracy and robustness than empirical models; however, they lack tangibly significant parameters [97]. They are also computationally complex, time-consuming, and unsuitable for engineering applications [96]. The research in this area can be further extended by applying other subsets of artificial intelligence techniques. Tables 6 and 7 summarize machine learning models used for gas-hydrate phase behavior studies and gas hydrate kinetics studies, respectively.

Table 6. Summary of machine learning models used for gas-hydrate phase behavior studies in the presence of chemical inhibitors.

Guest Component	Inhibitor	Model Type	References
C_1, C_2, C_3, *i*-C_4, *n*-C_4 CO_2, N, H_2S	MeOH, EG, EtOH, NaCl, $CaCl_2$	ANN	[164]
Natural gas	MeOH, EtOH, EG, DEG, TEG, salt	ANN	[177]

C_1, C_2, C_3, *i*-C_4, CO_2, N, H_2S	NaCl, KCl, $CaCl_2$, $MgCl_2$, MeOH, EG, DEG, TEG, 1-propanol, and 2-propanol, Glycerol	LSSVM	[178]
Natural gas	NaCl, KCl, $CaCl_2$, $MgCl_2$, MeOH, EG	LSSVM, Extra Trees (ET)	[179]
C_1, Natural gas	NaCl	ANN, SVM	[180]
Natural gas	NaCl, KCl, $CaCl_2$, $MgCl_2$	RF, ET, Extreme Gradient Boosting	[181]
C_1, C_2, C_3, *i*-C_4, N, H_2S, Mixed gas	NaCl, KCl, $CaCl_2$, $MgCl_2$, MeOH, EG, DEG, TEG, 1-propanol, and 2-propanol	AdaBoost-CART	[182]
C_1	NaCl, KCl, $CaCl_2$, $MgCl_2$	Multiple Linear Regression, SVM, RF, Gradient Boosting Regression	[183]
C_1, C_2, C_3, *i*-C_4, *i*-C_5, C_{6+}, CO_2, N, H_2S	NaCl, $CaCl_2$, MeOH	Extremely Randomized Trees	[184]

Table 7. Summary of machine learning models used for gas hydrate kinetics studies in the presence of chemical inhibitors.

Guest Component	Inhibitor	Model Type	References
Natural Gas	Polyvinylpyrrolidone (PVP)	ANN	[69]
C_1, C_3, *i*-C_4, CO_2	PVP, L-Tyrosine	ANN, ANFIS	[185]
C_1	Luvicap 55W	LSSVM, ANFIS, Gene Expression Programming	[186]

4.2.5. Quantum Chemistry-Based Modelling

The quantum chemistry-based model for designing, screening, and thermodynamic modelling of novel and developing solvents has been developed, and it has proven to be a useful predictive tool [97]. This tool is known as the conductor-like screening model for real solvents (COSMO-RS). COSMO-RS combines concepts derived from quantum chemistry and electrostatic interactions with statistical thermodynamics, providing a molecular-level link between quantum chemistry and chemical engineering thermodynamics [187]. Rapid thermodynamic calculations and solvent screening are made possible by this effective approach [188]. In this model, quantum chemistry calculations are performed, in which a molecule is placed inside a conductor, allowing the surface of the molecule to develop a charge distribution. This represents how the molecule would interact with a perfect conductor. The models make approximations, such as treating solvent effects using idealized conditions (e.g., perfect conductor approximation in COSMO-RS), which can lead to deviations from the experimental behavior. Furthermore, unlike regression-based models, quantum chemistry-based models do not incorporate experimental data during the calculation process, making them more prone to differences when applied to complex systems.

Chemical engineering research, pharmaceutical research for drug development, and the modelling of thermodynamic properties of ionic liquids are the main research areas where COSMO-RS has found its application [188,189]. Studies on carbon dioxide capture and solubility have reported using COSMO-RS as a screening method for ionic liquid characteristics [190,191]. COSMO-RS was introduced by Gonfa et al. [192] as a technique for adjusting ionic liquids for natural gas dehydration. Several researchers have used COSMO-RS to model pure deep eutectic solvents (DESs) and to forecast physical–chemical characteristics, including vapor pressure, density, heat capacity, and viscosity [193–195].

Claudio et al. [196] used COSMO-RS to estimate the ionic liquid's hydrogen bonding energies (E_{HB}), which are the energy exchanged during a hydrogen-bonding interaction between the accepter and donor of the ionic liquid. According to this study, COSMO-RS predicted E_{HB} to have a substantial correlation with experimental hydrogen bonding basicity. Hydrogen bonding basicity is known as the capacity of ionic liquids to take in hydrogen atoms [197]. Klamt [198] established the principle of interaction between water

and solute molecules using COSMO-RS to determine their sigma-profiles and sigma-potentials. In summary, COSMO-RS can be a useful tool for characterizing the water–solvent interactions of molecules, and hence it can be used to pre-screen ionic liquid hydrogen bonding basicity in gas hydrate applications [199]. To mitigate gas hydrates, Bavoh et al. [199] thus introduced COSMO-RS as a pre-screening technique for ionic liquids. The hydrogen-bonding energies (E_{HB}) of the investigated ionic liquids were predicted, and the impact of the predicted E_{HB} on the induction time and average depression temperature was examined. A discussion of the factors that influence the E_{HB} of ionic liquids was conducted, and a greater knowledge of the behaviors of ionic liquids in relation to water in terms of hydrogen bond donor and acceptor was presented. This was performed by establishing the sigma potential and sigma profile of the cations and anions of the investigated ionic liquids for gas hydrate inhibition.

The primary benefit of the COSMO-RS model is that it is prognostic in nature, and all that is needed to fit the model's parameters is the molecules' chemical structure, as no experimental data are required. However, a major limitation of this model is its qualitative agreement with the experimental data, which may result in low prediction accuracy [97]. The use of COSMO-RS for modelling and screening of gas hydrate inhibitors is still at infancy, and further work is so far required to select gas hydrate inhibitor candidates that are more effective by employing COSMO-RS. Table 8 summarizes a review of some previous studies that used the COSMO-RS modelling in the presence of chemical gas hydrate inhibitors.

Table 8. Summary of gas hydrate studies using COSMO-RS modelling in the presence of chemical gas hydrate inhibitors.

Guest Component	Inhibitor	Inhibitor Type	References
C_1	Ionic liquids	THI	[200]
C_1	Ionic liquids	THI/KHI	[199]
C_1	Ionic liquids	THI	[201]
CO_2	Amino acids	THI/KHI	[202]
C_1 and CO_2	Ionic liquids	THI	[203]
C_1	Amino acids, ionic liquids	KHI	[204]
C_1	Ionic liquids	THI	[205]
C_1	Ionic liquids	THI/KHI	[206]
C_1	DES	THI	[207]
C_1	Amino acids, ionic liquids	THI	[208]
C_1	Amino acids	THI/KHI	[209]
C_1	Ionic liquids	THI	[210]
C_1	Ionic liquids	THI	[211]

4.3. Comparison of Different Gas Hydrate Inhibition Models

The comparison of different models that have been discussed in this work is outlined in Table 9. In this summary, the strengths, limitations, and potential improvements required for the various modelling approaches are highlighted.

Table 9. Summary of strengths, limitations, and potential improvements of various modelling approaches reviewed in this work.

Model Approach	Strengths	Limitations	Potential Improvement
Empirical models	• Small number of input parameters, which enables quick prediction of the hydrate formation conditions.	• Large experimental data required. • Applicable to a few types of inhibitors.	• Development of models that are applicable to a wide variety of inhibitors.
Thermodynamic models	• High accuracy compared to kinetic models, and they are applicable in a wide temperature range. • Able to predict macroscopic properties such as pressure.	• Complexity in terms of programming and application. • Used in conjunction with time-consuming equations of state and mixing rules.	• Development of models that are accurate across a wide range of conditions relevant to industrial applications.
Kinetic models	• Offer a better understanding of the microscopic view of systems and their intrinsic behaviors as compared to thermodynamic models. • Form the basis for replicating experimental data within acceptable margins.	• Low accuracy due to the stochastic character of hydrate nucleation. • Not appropriate for real-time systems due to their reliance on experimental fitted parameters.	• Development of a unified model that can be accurately applicable on an industrial scale.
Machine learning models	• Have higher prediction accuracy and robustness than empirical models.	• Lack of tangibly significant parameters. • Computationally complex, time-consuming, and unsuitable for engineering applications.	• Extension of gas hydrate inhibition modelling to more subsets of artificial intelligence.
Quantum chemistry-based models	• Purely predictive, as no experimental data are required.	• Its qualitative agreement with experimental data results in low prediction accuracy.	• Integration of quantum chemistry-based models with machine learning techniques to enhance accuracy. • Incorporation of experimental data in a hybrid approach to minimize discrepancies between computed and observed values.

5. Conclusions and Future Perspectives

The development of accurate modelling techniques to predict the formation and dissociation conditions of gas hydrates in the presence of chemical inhibitors is very important, since experimental investigation is not always viable. This review article comprehensively summarizes the strides that have been made over the years in modelling gas hydrate chemical inhibition systems. Considerable advances in the development of accurate and reliable gas hydrate modelling approaches used in the context of chemical inhibition appear to be evident from the collection of studies reviewed in this article. The main features of the empirical models, thermodynamic models, kinetic models, machine learning models, and quantum chemistry-based models, typically the COSMO-RS model, are highlighted. Among the modelling techniques that have been presented in this review, the thermodynamic modelling approach seems to have been extended to several hydrate systems, as compared to other models, with the COSMO-RS being the novel approach. The introduction of this novel predictive technique is a significant step towards the development of screening tools for the analysis of un-synthesized inhibitors and the assessment of their industrial scale performance. Through the critical analysis process, the strengths

and limitations of each modelling approach have been highlighted. Given some of the limitations of these models, more research and development are still required in this area to improve the accuracy, predictive ability, and versatility of the fitted parameters across different conditions and systems, as well as the applicability of these models. The integration of quantum chemistry-based models with machine learning techniques to enhance predictive accuracy, as well as the incorporation of experimental data in this hybrid approach to minimize discrepancies between the computed and observed data, are potential future developments.

Furthermore, while the current focus of this article has been primarily on reviewing thermodynamic models, kinetic simulations such as molecular dynamics (MD) and numerical simulations have proven to be valuable tools in understanding how inhibitors affect the kinetics of hydrate formation and decomposition. This provides a more detailed insight into the underlying mechanisms that are often not accessible through experimental methods alone. MD simulations have been widely used to study the nucleation and growth of hydrate structures, as well as the interaction between hydrate inhibitors and guest molecules at the molecular level. Additionally, numerical hydrate simulations are valuable for scaling up molecular-level insights to real-world systems by simulating gas hydrate behavior in pipelines, reservoirs, and carbon sequestration processes. These simulators incorporate kinetic models to predict hydrate formation and dissociation rates under various conditions, which is essential for optimizing the use of inhibitors in gas transport and hydrate development applications. Considering the role of kinetic simulators, it is critical that a comprehensive review on this topic be conducted as part of future research to provide a meaningful overview of the methodologies used to study hydrate systems in the presence of inhibitors.

Author Contributions: Conceptualization, N.M.Z.; investigation, N.M.Z.; resources, K.T.; writing—original draft preparation, N.M.Z.; writing—review and editing, N.M.Z., K.T., and H.H.; visualization, N.M.Z.; supervision, K.T. and H.H.; project administration, K.T.; funding acquisition, K.T. and H.H. All authors have read and agreed to the published version of the manuscript.

Funding: This research received no external funding.

Data Availability Statement: No data were used.

Acknowledgments: This study has been supported by both Mangosuthu University of Technology and Witwatersrand University. Njabulo Mziwandile Zulu wishes to thank Mangosuthu University of Technology for the financial support while undertaking this research project.

Conflicts of Interest: The authors declare no conflicts of interest.

References

1. Hammerschmidt, E.G. Formation of Gas Hydrates in Natural Gas Transmission Lines. *Ind. Eng. Chem.* **1934**, *26*, 851–855. https://doi.org/10.1021/ie50296a010.
2. Huo, Z.; Freer, E.; Lamar, M.; Sannigrahi, B.; Knauss, D.M.; Sloan, E.D. Hydrate plug prevention by anti-agglomeration. *Chem. Eng. Sci.* **2001**, *56*, 4979–4991. https://doi.org/10.1016/S0009-2509(01)00188-9.
3. Wu, M.; Wang, S.; Liu, H. A Study on Inhibitors for the Prevention of Hydrate Formation in Gas Transmission Pipeline. *J. Nat. Gas Chem.* **2007**, *16*, 81–85. https://doi.org/10.1016/S1003-9953(07)60031-0.
4. Patel, Z.D.; Russum, J. Flow assurance: Chemical inhibition of gas hydrates in deepwater production systems. *Offshore* **2010**, *70*, 70–73.
5. Khan, M.S.; Lal, B.; Bustam, M.A. *Gas Hydrate Inhibitors*; Springer: Cham, Switzerland, 2020; ISBN 9783030307509. https://doi.org/10.1007/978-3-030-30750-9_2.
6. Lal, B.; Nashed, O. *Chemical Additives for Gas Hydrates*; Springer: Cham, Switzerland, 2020; ISBN 978-3-030-30749-3. https://10.1007/978-3-030-30750-9.
7. Sayani, J.K.S.; Lal, B.; Pedapati, S.R. *Comprehensive Review on Various Gas Hydrate Modelling Techniques: Prospects and Challenges*; Springer: Berlin/Heidelberg, Germany, 2022; Volume 29, ISBN 0123456789. https://doi.org/10.1007/s11831-021-09651-1.
8. Englezos, P. Clathrate hydrates. *Ind. Eng. Chem. Res.* **1993**, *32*, 1251–1274. https://doi.org/10.1021/ie00019a001.
9. Carroll, J.J. *Natural Gas Hydrates: A Guide for Engineers*; Gulf Professional Publishing: Houston, TX, USA, 2003; ISBN 9780750675697. https://doi.org/10.1016/B978-0-7506-7569-7.X5000-0.

10. Veluswamy, H.P.; Kumar, A.; Seo, Y.; Lee, J.D.; Linga, P. A review of solidified natural gas (SNG) technology for gas storage via clathrate hydrates. *Appl. Energy* **2018**, *216*, 262–285. https://doi.org/10.1016/j.apenergy.2018.02.059.
11. Sloan, E.D.; Koh, C.A. *Clathrate Hydrates of Natural Gases*, 3rd ed.; CRC Press: Boca Raton, FL, USA; Taylor & Francis Group: Abingdon, UK, 2008.
12. Carroll, J.J. *Natural Gas Hydrates: A Guide for Engineers*; Gulf Professional Publishing: Houston, TX, USA, 2009, Elsevier: Amsterdam, The Netherlands, 2009; ISBN 9780750684903.
13. Sloan, E.D. Gas Hydrates: Review of Physical/Chemical Properties. *Energy Fuels* **1998**, *12*, 191–196.
14. Shahnazar, S.; Hasan, N. Gas hydrate formation condition: Review on experimental and modeling approaches. *Fluid Phase Equilib.* **2014**, *379*, 72–85. https://doi.org/10.1016/j.fluid.2014.07.012.
15. Seo, Y.; Kang, S.-P. Inhibition of methane hydrate re-formation in offshore pipelines with a kinetic hydrate inhibitor. *J. Pet. Sci. Eng.* **2012**, *88–89*, 61–66. https://doi.org/10.1016/j.petrol.2011.11.001.
16. Majid, A.A.A.; Koh, C.A. Phase behavior and kinetics properties of gas hydrates in confinement and its application. *AIChE J.* **2021**, *67*, e17176. https://doi.org/10.1002/aic.17176.
17. Nkosi, N.; Nkazi, D.; Tumba, K. A review of thermodynamic and kinetic studies relevant to gas hydrate-based fruit juice concentration. *J. Food Eng.* **2023**, *341*, 111323. https://doi.org/10.1016/j.jfoodeng.2022.111323.
18. Jassim, E.; Abdi, M.A.; Muzychka, Y. A new approach to investigate hydrate deposition in gas-dominated flowlines. *J. Nat. Gas Sci. Eng.* **2010**, *2*, 163–177. https://doi.org/10.1016/j.jngse.2010.05.005.
19. Gaidukova, O.; Misyura, S.; Morozov, V.; Strizhak, P. Gas Hydrates: Applications and Advantages. *Energies* **2023**, *16*, 2866. https://doi.org/10.3390/en16062866.
20. Sami, N.A.; Sangwai, J.; Subramanian, B.; Sangwai, J.S.; Balasubramanian, N. Gas hydrate applications and problems in oil and gas industry. *Int. J. Sci. Eng. Res.* **2013**, *4*, 8. Available online: https://www.researchgate.net/profile/Nagham-Sami/publication/279188724_GAS_HYDRATE_APPLICATIONS_AND_PROBLEMS_IN_OIL_AND_GAS_INDUSTRY/links/558d408a08aee278cd38b6c7/GAS-HYDRATE-APPLICATIONS-AND-PROBLEMS-IN-OIL-AND-GAS-INDUSTRY.pdf (accessed on 4 March 2024).
21. Makogon, Y.F. Natural gas hydrates—A promising source of energy. *J. Nat. Gas Sci. Eng.* **2010**, *2*, 49–59. https://doi.org/10.1016/j.jngse.2009.12.004.
22. Eslamimanesh, A.; Mohammadi, A.H.; Richon, D.; Naidoo, P.; Ramjugernath, D. Application of gas hydrate formation in separation processes: A review of experimental studies. *J. Chem. Thermodyn.* **2012**, *46*, 62–71. https://doi.org/10.1016/J.JCT.2011.10.006.
23. Mesbah, M.; Abouali Galledari, S.; Soroush, E.; Momeni, M. Modeling Phase Behavior of Semi-Clathrate Hydrates of CO_2, CH_4, and N_2 in Aqueous Solution of Tetra-n-butyl Ammonium Fluoride. *J. Non-Equilib. Thermodyn.* **2019**, *44*, 155–167. https://doi.org/10.1515/jnet-2018-0079.
24. Matizakurima, F.; Babaee, S.; Hashemi, H.; Naidoo, P. Separation of Xenon from Noble Gas Mixtures of Argon, Krypton, and Xenon Using Gas Hydrate Technology. *Ind. Eng. Chem. Res.* **2023**, *62*, 14484–14496. https://doi.org/10.1021/acs.iecr.3c01174.
25. Eslamimanesh, A.; Mohammadi, A.H.; Richon, D. Thermodynamic model for predicting phase equilibria of simple clathrate hydrates of refrigerants. *Chem. Eng. Sci.* **2011**, *66*, 5439–5445. https://doi.org/10.1016/j.ces.2011.06.062.
26. Peng, X.; Hu, Y.; Liu, Y.; Jin, C.; Lin, H. Separation of ionic liquids from dilute aqueous solutions using the method based on CO_2 hydrates. *J. Nat. Gas Chem.* **2010**, *19*, 81–85. https://doi.org/10.1016/S1003-9953(09)60027-X.
27. Sloan, E.D. Natural Gas Hydrates. *J. Pet. Technol.* **1991**, *43*, 1414–1417. https://doi.org/10.2118/23562-pa.
28. Elhenawy, S.; Khraisheh, M.; Almomani, F.; Al-Ghouti, M.A.; Hassan, M.K.; Al-Muhtaseb, A. Towards Gas Hydrate-Free Pipelines: A Comprehensive Review of Gas Hydrate Inhibition Techniques. *Energies* **2022**, *15*, 8551. https://doi.org/10.3390/en15228551.
29. Nasir, Q.; Suleman, H.; Elsheikh, Y.A. A review on the role and impact of various additives as promoters/inhibitors for gas hydrate formation. *J. Nat. Gas Sci. Eng.* **2020**, *76*, 103211. https://doi.org/10.1016/j.jngse.2020.103211.
30. Semenov, A.P.; Mendgaziev, R.I.; Stoporev, A.S.; Istomin, V.A.; Sergeeva, D.V.; Tulegenov, T.B.; Vinokurov, V.A. Dimethyl sulfoxide as a novel thermodynamic inhibitor of carbon dioxide hydrate formation. *Chem. Eng. Sci.* **2022**, *255*, 117670. https://doi.org/10.1016/j.ces.2022.117670.
31. Englezos, P. Nucleation and Growth of Gas Hydrate Crystals in Relation to Kinetic Inhibition. *Rev. Inst. Français Pétrole* **1996**, *51*, 789–795. https://doi.org/10.2516/ogst:1996051.
32. Fu, S.B.; Cenegy, L.M.; Neff, C.S. A Summary of Successful Field Applications of A Kinetic Hydrate Inhibitor. In Proceedings of the SPE International Symposium on Oilfield Chemistry, Houston, TX, USA, 13–16 February 2001. https://doi.org/10.2118/65022-MS.
33. Yang, C.; Zi, M.; Wu, G.; Zou, X.; Liu, K.; Chen, D. Concentration effect of kinetic hydrate inhibitor on hydrate formation and inhibition. *Fuel* **2022**, *323*, 124448. https://doi.org/10.1016/j.fuel.2022.124448.
34. Aman, Z.M.; Koh, C.A. Interfacial phenomena in gas hydrate systems. *Chem. Soc. Rev.* **2016**, *45*, 1678–1690. https://doi.org/10.1039/C5CS00791G.
35. Tohidi, B.; Anderson, R.; Mozaffar, H.; Tohidi, F. The Return of Kinetic Hydrate Inhibitors. *Energy Fuels* **2015**, *29*, 8254–8260. https://doi.org/10.1021/acs.energyfuels.5b01794.
36. Xiao, C.; Adidharma, H. Dual function inhibitors for methane hydrate. *Chem. Eng. Sci.* **2009**, *64*, 1522–1527. https://doi.org/10.1016/j.ces.2008.12.031.

37. Xiao, C.; Wibisono, N.; Adidharma, H. Dialkylimidazolium halide ionic liquids as dual function inhibitors for methane hydrate. *Chem. Eng. Sci.* **2010**, *65*, 3080–3087. https://doi.org/10.1016/j.ces.2010.01.033.
38. Chen, Q.; Yu, Y.; Zeng, P.; Yang, W.; Liang, Q.; Peng, X.; Liu, Y.; Hu, Y. Effect of 1-butyl-3-methylimidazolium tetrafluoroborate on the formation rate of CO_2 hydrate. *J. Nat. Gas Chem.* **2008**, *17*, 264–267. https://doi.org/10.1016/S1003-9953(08)60061-4.
39. Richon, D. New experimental developments for phase equilibrium measurements. *Fluid Phase Equilib.* **1996**, *116*, 421–428. https://doi.org/10.1016/0378-3812(95)02914-1.
40. Oellrich, L. Natural gas hydrates and their potential for future energy supply. In Proceedings of the 6th ISHMT/ASME Heat and Mass Transfer Conference, Kalpakkam, India, 5–7 January 2004; pp. 70–78.
41. Hashemi, H. Application of Gas Hydrates in Cold Storage Technology: Experimental Study and Thermodynamic Modeling. Ph.D. Thesis, University of KwaZulu-Natal, Durban, South Africa, 2015.
42. Mohammadi, A.H.; Tohidi, B.; Burgass, R.W. Equilibrium Data and Thermodynamic Modeling of Nitrogen, Oxygen, and Air Clathrate Hydrates. *J. Chem. Eng. Data* **2003**, *48*, 612–616. https://doi.org/10.1021/je025608x.
43. Ke, W.; Kelland, M.A. Kinetic Hydrate Inhibitor Studies for Gas Hydrate Systems: A Review of Experimental Equipment and Test Methods. *Energy Fuels* **2016**, *30*, 10015–10028. https://doi.org/10.1021/acs.energyfuels.6b02739.
44. Wylde, J.; Bodnar, S.; Mazzeo, C.; Ward, Z. Preventing gas hydrate plugging in deepwater wells. *World Oil* **2021**, *242*, 59–63.
45. Dalmazzone, D.; Kharrat, M.; Lachet, V.; Fouconnier, B.; Clausse, D. DSC and PVT measurements. *J. Therm. Anal. Calorim.* **2002**, *70*, 493–505.
46. Salmin, D.C.; Estanga, D.; Koh, C.A. Review of gas hydrate anti-agglomerant screening techniques. *Fuel* **2022**, *319*, 122862. https://doi.org/10.1016/j.fuel.2021.122862.
47. Tariq, M.; Rooney, D.; Othman, E.; Aparicio, S.; Atilhan, M.; Khraisheh, M. Gas hydrate inhibition: A review of the role of ionic liquids. *Ind. Eng. Chem. Res.* **2014**, *53*, 17855–17868. https://doi.org/10.1021/ie503559k.
48. Khan, M.S.; Bavoh, C.B.; Partoon, B.; Lal, B.; Bustam, M.A.; Shariff, A.M. Thermodynamic effect of ammonium based ionic liquids on CO_2 hydrates phase boundary. *J. Mol. Liq.* **2017**, *238*, 533–539. https://doi.org/10.1016/j.molliq.2017.05.045.
49. Tumba, K.; Reddy, P.; Naidoo, P.; Ramjugernath, D.; Eslamimanesh, A.; Mohammadi, A.H.; Richon, D. Phase equilibria of methane and carbon dioxide clathrate hydrates in the presence of aqueous solutions of tributylmethylphosphonium methylsulfate ionic liquid. *J. Chem. Eng. Data* **2011**, *56*, 3620–3629. https://doi.org/10.1021/je200462q.
50. Kazemi, F.; Javanmardi, J.; Aftab, S.; Mohammadi, A.H. Experimental study and thermodynamic modeling of the stability conditions of methane clathrate hydrate in the presence of TEACl and/or BMIM-BF4 in aqueous solution. *J. Chem. Thermodyn.* **2019**, *130*, 95–103. https://doi.org/10.1016/j.jct.2018.09.014.
51. Khan, M.S.; Bavoh, C.B.; Partoon, B.; Nashed, O.; Lal, B.; Mellon, N.B. Impacts of ammonium based ionic liquids alkyl chain on thermodynamic hydrate inhibition for carbon dioxide rich binary gas. *J. Mol. Liq.* **2018**, *261*, 283–290. https://doi.org/10.1016/j.molliq.2018.04.015.
52. Sa, J.-H.; Kwak, G.-H.; Han, K.; Ahn, D.; Cho, S.J.; Lee, J.D.; Lee, K.-H. Inhibition of methane and natural gas hydrate formation by altering the structure of water with amino acids. *Sci. Rep.* **2016**, *6*, 31582. https://doi.org/10.1038/srep31582.
53. Li, X.S.; Liu, Y.J.; Zeng, Z.Y.; Chen, Z.Y.; Li, G.; Wu, H.J. Equilibrium hydrate formation conditions for the mixtures of methane + ionic liquids + water. *J. Chem. Eng. Data* **2011**, *56*, 119–123. https://doi.org/10.1021/je100987q.
54. Zare, M.; Haghtalab, A.; Ahmadi, A.N.; Nazari, K. Experiment and thermodynamic modeling of methane hydrate equilibria in the presence of aqueous imidazolium-based ionic liquid solutions using electrolyte cubic square well equation of state. *Fluid Phase Equilib.* **2013**, *341*, 61–69. https://doi.org/10.1016/j.fluid.2012.12.024.
55. Richard, A.R.; Adidharma, H. The performance of ionic liquids and their mixtures in inhibiting methane hydrate formation. *Chem. Eng. Sci.* **2013**, *87*, 270–276. https://doi.org/10.1016/j.ces.2012.10.021.
56. Partoon, B.; Wong, N.M.S.; Sabil, K.M.; Nasrifar, K.; Ahmad, M.R. A study on thermodynamics effect of [EMIM]-Cl and [OH-C2MIM]-Cl on methane hydrate equilibrium line. *Fluid Phase Equilib.* **2013**, *337*, 26–31. https://doi.org/10.1016/j.fluid.2012.09.025.
57. Lee, D.; Go, W.; Ko, G.; Seo, Y. Inhibition synergism of glycine (an amino acid) and [BMIM][BF4] (an ionic liquid) on the growth of CH_4 hydrate. *Chem. Eng. J.* **2020**, *393*, 124466. https://doi.org/10.1016/j.cej.2020.124466.
58. Del Villano, L.; Kelland, M.A. An investigation into the kinetic hydrate inhibitor properties of two imidazolium-based ionic liquids on Structure II gas hydrate. *Chem. Eng. Sci.* **2010**, *65*, 5366–5372. https://doi.org/10.1016/j.ces.2010.06.033.
59. Abay, H.K.; Svartaas, T.M.; Ke, W. Effect of Gas Composition on sII Hydrate Growth Kinetics. *Energy Fuels* **2011**, *25*, 1335–1341. https://doi.org/10.1021/ef101698g.
60. O'Reilly, R.; Ieong, N.S.; Chua, P.C.; Kelland, M.A. Missing Poly(N-vinyl lactam) Kinetic Hydrate Inhibitor: High-Pressure Kinetic Hydrate Inhibition of Structure II Gas Hydrates with Poly(N-vinyl piperidone) and Other Poly(N-vinyl lactam) Homopolymers. *Energy Fuels* **2011**, *25*, 4595–4599. https://doi.org/10.1021/ef2009953.
61. Rasoolzadeh, A.; Javanmardi, J.; Eslamimanesh, A.; Mohammadi, A.H. Experimental study and modeling of methane hydrate formation induction time in the presence of ionic liquids. *J. Mol. Liq.* **2016**, *221*, 149–155. https://doi.org/10.1016/j.molliq.2016.05.016.
62. Duchateau, C.; Peytavy, J.-L.; Glénat, P.; Pou, T.-E.; Hidalgo, M.; Dicharry, C. Laboratory Evaluation of Kinetic Hydrate Inhibitors: A Procedure for Enhancing the Repeatability of Test Results. *Energy Fuels* **2009**, *23*, 962–966. https://doi.org/10.1021/ef800710x.
63. Jensen, L.; Thomsen, K.; von Solms, N. Inhibition of Structure I and II Gas Hydrates Using Synthetic and Biological Kinetic Inhibitors. *Energy Fuels* **2011**, *25*, 17–23. https://doi.org/10.1021/ef100833n.

64. Xu, Y.; Yang, M.; Yang, X. Chitosan as green kinetic inhibitors for gas hydrate formation. *J. Nat. Gas Chem.* **2010**, *19*, 431–435. https://doi.org/10.1016/S1003-9953(09)60083-9.
65. Kumar, A.; Sakpal, T.; Kumar, R. Influence of Low-Dosage Hydrate Inhibitors on Methane Clathrate Hydrate Formation and Dissociation Kinetics. *Energy Technol.* **2015**, *3*, 717–725. https://doi.org/10.1002/ente.201500004.
66. Lee, W.; Shin, J.-Y.; Kim, K.-S.; Kang, S.-P. Kinetic Promotion and Inhibition of Methane Hydrate Formation by Morpholinium Ionic Liquids with Chloride and Tetrafluoroborate Anions. *Energy Fuels* **2016**, *30*, 3879–3885. https://doi.org/10.1021/acs.energyfuels.6b00271.
67. Xu, S.; Fan, S.; Wang, Y.; Lang, X. An Investigation of Kinetic Hydrate Inhibitors on the Natural Gas from the South China Sea. *J. Chem. Eng. Data* **2015**, *60*, 311–318. https://doi.org/10.1021/je500600t.
68. Sharifi, H.; Englezos, P. Accelerated Hydrate Crystal Growth in the Presence of Low Dosage Additives Known as Kinetic Hydrate Inhibitors. *J. Chem. Eng. Data* **2015**, *60*, 336–342. https://doi.org/10.1021/je500591q.
69. Daraboina, N.; Ripmeester, J.; Walker, V.K.; Englezos, P. Natural Gas Hydrate Formation and Decomposition in the Presence of Kinetic Inhibitors. 1. High Pressure Calorimetry. *Energy Fuels* **2011**, *25*, 4392–4397. https://doi.org/10.1021/ef200812m.
70. Chua, P.C.; Kelland, M.A. Study of the Gas Hydrate Antiagglomerant Performance of a Series of Mono-and Bis-amine Oxides: Dual Antiagglomerant and Kinetic Hydrate Inhibition Behavior. *Energy Fuels* **2018**, *32*, 1674–1684. https://doi.org/10.1021/acs.energyfuels.7b03789.
71. Hu, S.; Vo, L.; Monteiro, D.; Bodnar, S.; Prince, P.; Koh, C.A. Structural Effects of Gas Hydrate Antiagglomerant Molecules on Interfacial Interparticle Force Interactions. *Langmuir* **2021**, *37*, 1651–1661. https://doi.org/10.1021/acs.langmuir.0c02503.
72. Costa Salmin, D.; Delgado-Linares, J.; Wu, D.T.; Zerpa, L.E.; Koh, C.A. Hydrate Agglomeration in Crude Oil Systems in Which the Asphaltene Aggregation State is Artificially Modified. *SPE J.* **2021**, *26*, 1189–1199. https://doi.org/10.4043/29484-MS.
73. De Menezes, D.É.S.; Filho, P.d.A.P.; Fuentes, M.D.R. Use of 1-butyl-3-methylimidazolium-based ionic liquids as methane hydrate inhibitors at high pressure conditions. *Chem. Eng. Sci.* **2020**, *212*, 115323. https://doi.org/10.1016/j.ces.2019.115323.
74. Lee, D.; Go, W.; Seo, Y. Experimental and computational investigation of methane hydrate inhibition in the presence of amino acids and ionic liquids. *Energy* **2019**, *182*, 632–640. https://doi.org/10.1016/j.energy.2019.06.025.
75. Khan, M.S.; Lal, B.; Shariff, A.M.; Mukhtar, H. Ammonium hydroxide ILs as dual-functional gas hydrate inhibitors for binary mixed gas (carbon dioxide and methane) hydrates. *J. Mol. Liq.* **2019**, *274*, 33–44. https://doi.org/10.1016/j.molliq.2018.10.076.
76. Tohidi, B.; Burgass, R.W.; Danesh, A.; Østergaard, K.K.; Todd, A.C. Improving the accuracy of gas hydrate dissociation point measurements. *Ann. New York Acad. Sci. USA* **2000**, *912*, 924–931. https://doi.org/10.1111/j.1749-6632.2000.tb06846.x.
77. Dohrn, R.; Fonseca, J.M.S.; Peper, S. Experimental Methods for Phase Equilibria at High Pressures. *Annu. Rev. Chem. Biomol. Eng.* **2012**, *3*, 343–367. https://doi.org/10.1146/annurev-chembioeng-062011-081008.
78. Ohmura, R.; Takeya, S.; Uchida, T.; Ebinuma, T. Clathrate hydrate formed with methane and 2-propanol: Confirmation of structure II hydrate formation. *Ind. Eng. Chem. Res.* **2004**, *43*, 4964–4966. https://doi.org/10.1021/ie0498089.
79. Mohammad-Taheri, M.; Zarringhalam Moghaddam, A.; Nazari, K.; Gholipour Zanjani, N. The role of thermal path on the accuracy of gas hydrate phase equilibrium data using isochoric method. *Fluid Phase Equilib.* **2013**, *338*, 257–264. https://doi.org/10.1016/j.fluid.2012.10.010.
80. Cha, M.; Shin, K.; Kim, J.; Chang, D.; Seo, Y.; Lee, H.; Kang, S.-P. Thermodynamic and kinetic hydrate inhibition performance of aqueous ethylene glycol solutions for natural gas. *Chem. Eng. Sci.* **2013**, *99*, 184–190. https://doi.org/10.1016/j.ces.2013.05.060.
81. Bavoh, C.B.; Partoon, B.; Lal, B.; Kok Keong, L. Methane hydrate-liquid-vapour-equilibrium phase condition measurements in the presence of natural amino acids. *J. Nat. Gas Sci. Eng.* **2017**, *37*, 425–434. https://doi.org/10.1016/j.jngse.2016.11.061.
82. Nashed, O.; Dadebayev, D.; Khan, M.S.; Bavoh, C.B.; Lal, B.; Shariff, A.M. Experimental and modelling studies on thermodynamic methane hydrate inhibition in the presence of ionic liquids. *J. Mol. Liq.* **2018**, *249*, 886–891. https://doi.org/10.1016/j.molliq.2017.11.115.
83. Tavasoli, H.; Feyzi, F.; Dehghani, M.R.; Alavi, F. Prediction of gas hydrate formation condition in the presence of thermodynamic inhibitors with the Elliott–Suresh–Donohue Equation of State. *J. Pet. Sci. Eng.* **2011**, *77*, 93–103. https://doi.org/10.1016/j.petrol.2011.02.002.
84. Mohammadi, A.H.; Tohidi, B. A Novel Predictive Technique for Estimating the Hydrate Inhibition Effects of Single and Mixed Thermodynamic Inhibitors. *Can. J. Chem. Eng.* **2005**, *83*, 951–961. https://doi.org/10.1002/cjce.5450830604.
85. Hu, Y.; Lee, B.R.; Sum, A.K. Universal correlation for gas hydrates suppression temperature of inhibited systems: I. Single salts. *AIChE J.* **2017**, *63*, 5111–5124. https://doi.org/10.1002/aic.15846.
86. Carroll, J.J. *Natural Gas Hydrates: A Guide for Engineers*; Chapter 3 Hand Calculation Methods; Gulf Professional Publishing: Houston, TX, USA, 2014; ISBN 008057002X.
87. Nielsen, R.B.; Bucklin, R.W. Why not Use Methanol for Hydrate Control? *Hydrocarb. Process.* **1983**, *62*, 71–78.
88. Sira, J.H.; Patil, S.L.; Kamath, V.A. Study of Hydrate Dissociation by Methanol and Glycol Injection. In Proceedings of the SPE Annual Technical Conference and Exhibition, New Orleans, LA, USA, 23–26 September 1990. https://doi.org/10.2118/20770-MS.
89. McCain, W.D. Reservoir-Fluid Property Correlations—State of the Art. *SPE Reserv. Eng.* **1991**, *6*, 266–272. https://doi.org/10.2118/18571-PA.
90. Yousif, M.H.; Young, D.B. A Simple Correlation To Predict the Hydrate Point Suppression in Drilling Fluids. In Proceedings of the SPE/IADC Drilling Conference, Amsterdam, The Netherlands, 22–25 February 1993.

91. Østergaard, K.K.; Masoudi, R.; Tohidi, B.; Danesh, A.; Todd, A.C. A general correlation for predicting the suppression of hydrate dissociation temperature in the presence of thermodynamic inhibitors. *J. Pet. Sci. Eng.* **2005**, *48*, 70–80. https://doi.org/10.1016/j.petrol.2005.04.002.
92. Najibi, H.; Mohammadi, A.H.; Tohidi, B. Estimating the Hydrate Safety Margin in the Presence of Salt and/or Organic Inhibitor Using Freezing Point Depression Data of Aqueous Solutions. *Ind. Eng. Chem. Res.* **2006**, *45*, 4441–4446. https://doi.org/10.1021/ie051265v.
93. Bahadori, A.; Vuthaluru, H.B.; Mokhatab, S.; Tade, M.O. Predicting hydrate forming pressure of pure alkanes in the presence of inhibitors. *J. Nat. Gas Chem.* **2008**, *17*, 249–255. https://doi.org/10.1016/S1003-9953(08)60059-6.
94. Aregbe, A.G. A Generalized Correlation for Predicting Ethane, Propane, and Isobutane Hydrates Equilibrium Data in Pure Water and Aqueous Salt Solutions. *Glob. Challenges* **2019**, *3*, 1800069. https://doi.org/10.1002/gch2.201800069.
95. Mohamadi-Baghmolaei, M.; Hajizadeh, A.; Azin, R.; Izadpanah, A.A. Assessing thermodynamic models and introducing novel method for prediction of methane hydrate formation. *J. Pet. Explor. Prod. Technol.* **2018**, *8*, 1401–1412. https://doi.org/10.1007/s13202-017-0415-2.
96. Zhang, G.; Li, J.; Liu, G.; Yang, H.; Huang, H. Applicability research of thermodynamic models of gas hydrate phase equilibrium based on different equations of state. *RSC Adv.* **2022**, *12*, 15870–15884. https://doi.org/10.1039/D2RA00875K.
97. Alkhatib, I.I.I.; Bahamon, D.; Llovell, F.; Abu-Zahra, M.R.M.; Vega, L.F. Perspectives and guidelines on thermodynamic modelling of deep eutectic solvents. *J. Mol. Liq.* **2020**, *298*, 112183. https://doi.org/10.1016/j.molliq.2019.112183.
98. Van der Waals, J.H.; Platteeuw, J.C. Clathrate Solutions. In *Advances in Chemical Physics*; Wiley: Hoboken, NJ, USA, 1959; Volume 2.
99. Saito, S.; Marshall, D.R.; Kobayashi, R. Hydrates at high pressures: Part II. Application of statistical mechanics to the study of the hydrates of methane, argon, and nitrogen. *AIChE J.* **1964**, *10*, 734–740. https://doi.org/10.1002/aic.690100530.
100. Parrish, W.R.; Prausnitz, J.M. Dissociation Pressures of Gas Hydrates Formed by Gas Mixtures. *Ind. Eng. Chem. Process Des. Dev.* **1972**, *11*, 26–35. https://doi.org/10.1021/i260041a006.
101. Holder, G.D.; Corbin, G.; Papadopoulos, K.D. Thermodynamic and Molecular Properties of Gas Hydrates from Mixtures Containing Methane, Argon, and Krypton. *Ind. Eng. Chem. Fundam.* **1980**, *19*, 282–286. https://doi.org/10.1021/i160075a008.
102. Holder, G.D.; Zetts, S.P.; Pradhan, N. Phase behavior in systems containing clathrate hydrates: A review. *Rev. Chem. Eng.* **1988**, *5*, 1–70. https://doi.org/10.1515/REVCE.1988.5.1-4.1.
103. John, V.T.; Holder, G.D. Choice of cell size in the cell theory of hydrate phase gas-water interactions. *J. Phys. Chem.* **1981**, *85*, 1811–1814. https://doi.org/10.1021/j150613a010.
104. John, V.T.; Holder, G.D. Contribution of second and subsequent water shells to the potential energy of guest-host interactions in clathrate hydrates. *J. Phys. Chem.* **1982**, *86*, 455–459. https://doi.org/10.1021/j100393a008.
105. John, V.T.; Holder, G.D. Langmuir constants for spherical and linear molecules in clathrate hydrates. Validity of the cell theory. *J. Phys. Chem.* **1985**, *89*, 3279–3285. https://doi.org/10.1021/j100261a023.
106. John, V.T.; Papadopoulos, K.D.; Holder, G.D. A generalized model for predicting equilibrium conditions for gas hydrates. *AIChE J.* **1985**, *31*, 252–259. https://doi.org/10.1002/aic.690310212.
107. Wang, L.B.; Cui, J.L.; Sun, C.Y.; Ma, Q.L.; Fan, S.S.; Wang, X.H.; Chen, G.J. Review on the applications and modifications of the chen-guo model for hydrate formation and dissociation. *Energy Fuels* **2021**, *35*, 2936–2964. https://doi.org/10.1021/acs.energyfuels.0c03977.
108. Chen, G.J.; Guo, T.M. Thermodynamic modeling of hydrate formation based on new concepts. *Fluid Phase Equilib.* **1996**, *122*, 43–65. https://doi.org/10.1016/0378-3812(96)03032-4.
109. Chen, G.-J.; Guo, T.-M. A new approach to gas hydrate modelling. *Chem. Eng. J.* **1998**, *71*, 145–151. https://doi.org/10.1016/S1385-8947(98)00126-0.
110. Esmaeilzadeh, F.; Hamedi, N.; Karimipourfard, D.; Rasoolzadeh, A. An insight into the role of the association equations of states in gas hydrate modeling: A review. *Pet. Sci.* **2020**, *17*, 1432–1450. https://doi.org/10.1007/s12182-020-00471-9.
111. Klauda, J.B.; Sandler, S.I. A Fugacity Model for Gas Hydrate Phase Equilibria. *Ind. Eng. Chem. Res.* **2000**, *39*, 3377–3386. https://doi.org/10.1021/ie000322b.
112. McMullan, R.K.; Jeffrey, G.A. Polyhedral Clathrate Hydrates. IX. Structure of Ethylene Oxide Hydrate. *J. Chem. Phys.* **1965**, *42*, 2725–2732. https://doi.org/10.1063/1.1703228.
113. Larsen, B.L.; Rasmussen, P.; Fredenslund, A. A modified UNIFAC group-contribution model for prediction of phase equilibria and heats of mixing. *Ind. Eng. Chem. Res.* **1987**, *26*, 2274–2286. https://doi.org/10.1021/ie00071a018.
114. Garapati, N.; Anderson, B.J. Statistical thermodynamics model and empirical correlations for predicting mixed hydrate phase equilibria. *Fluid Phase Equilib.* **2014**, *373*, 20–28. https://doi.org/10.1016/j.fluid.2014.03.010.
115. Jager, M..; Sloan, E.. The effect of pressure on methane hydration in pure water and sodium chloride solutions. *Fluid Phase Equilib.* **2001**, *185*, 89–99. https://doi.org/10.1016/S0378-3812(01)00459-9.
116. Li, X.-S.; Wu, H.-J.; Englezos, P. Prediction of Gas Hydrate Formation Conditions in the Presence of Methanol, Glycerol, Ethylene Glycol, and Triethylene Glycol with the Statistical Associating Fluid Theory Equation of State. *Ind. Eng. Chem. Res.* **2006**, *45*, 2131–2137. https://doi.org/10.1021/ie051204x.
117. Jiang, H.; Adidharma, H. Thermodynamic modeling of aqueous ionic liquid solutions and prediction of methane hydrate dissociation conditions in the presence of ionic liquid. *Chem. Eng. Sci.* **2013**, *102*, 24–31. https://doi.org/10.1016/j.ces.2013.07.049.

118. Chapoy, A.; Burgass, R.; Tohidi, B.; Alsiyabi, I. Hydrate and Phase Behavior Modeling in CO_2-Rich Pipelines. *J. Chem. Eng. Data* **2015**, *60*, 447–453. https://doi.org/10.1021/je500834t.
119. Kondori, J.; Zendehboudi, S.; James, L. Evaluation of Gas Hydrate Formation Temperature for Gas/Water/Salt/Alcohol Systems: Utilization of Extended UNIQUAC Model and PC-SAFT Equation of State. *Ind. Eng. Chem. Res.* **2018**, *57*, 13833–13855. https://doi.org/10.1021/acs.iecr.8b03011.
120. Ma, Q.-L.; Chen, G.-J.; Guo, T.-M. Modelling the gas hydrate formation of inhibitor containing systems. *Fluid Phase Equilib.* **2003**, *205*, 291–302. https://doi.org/10.1016/S0378-3812(02)00295-9.
121. Delavar, H.; Haghtalab, A. Prediction of hydrate formation conditions using GE-EOS and UNIQUAC models for pure and mixed-gas systems. *Fluid Phase Equilib.* **2014**, *369*, 1–12. https://doi.org/10.1016/j.fluid.2014.02.009.
122. Delavar, H.; Haghtalab, A. Thermodynamic modeling of gas hydrate formation conditions in the presence of organic inhibitors, salts and their mixtures using UNIQUAC model. *Fluid Phase Equilib.* **2015**, *394*, 101–117. https://doi.org/10.1016/j.fluid.2015.03.008.
123. Ahmadian, S.; Mohammadi, M.; Ehsani, M.R. Thermodynamic modeling of methane hydrate formation in the presence of imidazolium-based ionic liquids using two-step hydrate formation theory and CPA EoS. *Fluid Phase Equilib.* **2018**, *474*, 32–42. https://doi.org/10.1016/j.fluid.2018.07.004.
124. Li, S.; Li, Y.; Yang, L.; Han, Y.; Jiang, Z. Prediction of equilibrium conditions for gas hydrates in the organic inhibitor aqueous solutions using a thermodynamic consistency-based model. *Fluid Phase Equilib.* **2021**, *544–545*, 113118. https://doi.org/10.1016/j.fluid.2021.113118.
125. Mu, L.; Li, X.; Tan, Q.; Zhou, Z.; Zhao, H.; Cui, Q. Thermodynamic modeling of gas hydrate phase equilibrium conditions in porous media in the presence of inhibitor solution. *Fluid Phase Equilib.* **2023**, *568*, 113752. https://doi.org/10.1016/j.fluid.2023.113752.
126. Chin, H.-Y.; Lee, B.-S.; Chen, Y.-P.; Chen, P.-C.; Lin, S.-T.; Chen, L.-J. Prediction of Phase Equilibrium of Methane Hydrates in the Presence of Ionic Liquids. *Ind. Eng. Chem. Res.* **2013**, *52*, 16985–16992. https://doi.org/10.1021/ie4027023.
127. Dongre, H.J.; Jana, A.K. Insight into the thermo-physics of gas hydrates: Three phase equilibrium in presence of electrolyte. *J. Chem. Thermodyn.* **2020**, *150*, 106182. https://doi.org/10.1016/j.jct.2020.106182.
128. Sarkhel, R.; Sahu, C.; Kumar, R.; Sangwai, J.S. Effects of sodium hydroxide and calcium hydroxide on the phase equilibria of methane hydrates. *J. Chem. Thermodyn.* **2023**, *177*, 106935. https://doi.org/10.1016/j.jct.2022.106935.
129. Dehbandi Baladehi, M.; Kamran-Pirzaman, A.; Mohammad-Taheri, M.; Taheri Rizi, Z.; Aminolroayaei, M.A. Thermodynamic modeling of sour gas mixture (CH_4/C_3H_8/H_2S) hydrate formation in the presence of thermodynamic inhibitors mono ethylene glycol, NaCl, and $CaCl_2$ using the ion pair concept. *Pet. Sci. Technol.* **2024**, 1–23. https://doi.org/10.1080/10916466.2024.2337400.
130. Bishnoi, P.R.; Natarajan, V. Formation and decomposition of gas hydrates. *Fluid Phase Equilib.* **1996**, *117*, 168–177. https://doi.org/10.1016/0378-3812(95)02950-8.
131. Yin, Z.; Khurana, M.; Tan, H.K.; Linga, P. A review of gas hydrate growth kinetic models. *Chem. Eng. J.* **2018**, *342*, 9–29. https://doi.org/10.1016/j.cej.2018.01.120.
132. Li, B.; Li, X.-S.; Li, G. Kinetic studies of methane hydrate formation in porous media based on experiments in a pilot-scale hydrate simulator and a new model. *Chem. Eng. Sci.* **2014**, *105*, 220–230. https://doi.org/10.1016/j.ces.2013.11.016.
133. Li, S.; Sun, C.; Liu, B.; Feng, X.; Li, F.; Chen, L.; Chen, G. Initial thickness measurements and insights into crystal growth of methane hydrate film. *AIChE J.* **2013**, *59*, 2145–2154. https://doi.org/10.1002/aic.13987.
134. Makogon, Y.F. *Hydrates of Natural Gas*; Pennwell Corp: Tulsa, OK, USA, 1981.
135. Kvamme, B.; Graue, A.; Aspenes, E.; Kuznetsova, T.; Gránásy, L.; Tóth, G.; Pusztai, T.; Tegze, G. Kinetics of solid hydrate formation by carbon dioxide: Phase field theory of hydrate nucleation and magnetic resonance imaging. *Phys. Chem. Chem. Phys.* **2004**, *6*, 2327–2334. https://doi.org/10.1039/B311202K.
136. Englezos, P.; Kalogerakis, N.; Dholabhai, P.D.; Bishnoi, P.R. Kinetics of formation of methane and ethane gas hydrates. *Chem. Eng. Sci.* **1987**, *42*, 2647–2658. https://doi.org/10.1016/0009-2509(87)87015-X.
137. Ribeiro, C.P.; Lage, P.L.C. Modelling of hydrate formation kinetics: State-of-the-art and future directions. *Chem. Eng. Sci.* **2008**, *63*, 2007–2034. https://doi.org/10.1016/j.ces.2008.01.014.
138. Dholabhai, P.D.; Kalogerakis, N.; Bishnoi, P.R. Kinetics of methane hydrate formation in aqueous electrolyte solutions. *Can. J. Chem. Eng.* **1993**, *71*, 68–74. https://doi.org/10.1002/cjce.5450710110.
139. Malegaonkar, M.B.; Dholabhai, P.D.; Bishnoi, P.R. Kinetics of carbon dioxide and methane hydrate formation. *Can. J. Chem. Eng.* **1997**, *75*, 1090–1099. https://doi.org/10.1002/cjce.5450750612.
140. Skovborg, P.; Rasmussen, P. A mass transport limited model for the growth of methane and ethane gas hydrates. *Chem. Eng. Sci.* **1994**, *49*, 1131–1143. https://doi.org/10.1016/0009-2509(94)85085-2.
141. Herri, J.M.; Pic, J.S.; Gruy, F.; Cournil, M. Methane hydrate crystallization mechanism from in-situ particle sizing. *AIChE J.* **1999**, *45*, 590–602. https://doi.org/10.1002/aic.690450316.
142. Christiansen, R.L.; Bansal, V.; Sloan, E.D. Avoiding Hydrates in the Petroleum Industry: Kinetics of Formation. In Proceedings of the SPE University of Tulsa Centennial Petroleum Engineering Symposium, Tulsa, OK, USA, 29–31 August 1994. https://doi.org/10.2118/27994-MS.
143. Natarajan, V.; Bishnoi, P.R.; Kalogerakis, N. Induction phenomena in gas hydrate nucleation. *Chem. Eng. Sci.* **1994**, *49*, 2075–2087. https://doi.org/10.1016/0009-2509(94)E0026-M.

144. Kang, S.-P.; Shin, J.-Y.; Lim, J.-S.; Lee, S. Experimental measurement of the induction time of natural gas Hydrate and its prediction with polymeric kinetic inhibitor. *Chem. Eng. Sci.* **2014**, *116*, 817–823. https://doi.org/10.1016/j.ces.2014.04.035.
145. Kashchiev, D.; Firoozabadi, A. Induction time in crystallization of gas hydrates. *J. Cryst. Growth* **2003**, *250*, 499–515. https://doi.org/10.1016/S0022-0248(02)02461-2.
146. Talaghat, M.R.; Jokar, S.M. Prediction of induction time for methane hydrate formation in the presence or absence of THF in flow loop system by Natarajan model. *Heat Mass Transf.* **2018**, *54*, 2783–2792. https://doi.org/10.1007/s00231-017-2263-5.
147. Natarajan, V. *Thermodynamics and Nucleation Kinetics of Gas Hydrates*; Elsevier: Amsterdam, The Netherlands, 1996.
148. Roosta, H.; Dashti, A.; Mazloumi, S.H.; Varaminian, F. Inhibition properties of new amino acids for prevention of hydrate formation in carbon dioxide–water system: Experimental and modeling investigations. *J. Mol. Liq.* **2016**, *215*, 656–663. https://doi.org/10.1016/j.molliq.2016.01.039.
149. Roosta, H.; Khosharay, S.; Varaminian, F. Experimental study of methane hydrate formation kinetics with or without additives and modeling based on chemical affinity. *Energy Convers. Manag.* **2013**, *76*, 499–505. https://doi.org/10.1016/j.enconman.2013.05.024.
150. Kar, S.; Kakati, H.; Mandal, A.; Laik, S. Experimental and modeling study of kinetics for methane hydrate formation in a crude oil-in-water emulsion. *Pet. Sci.* **2016**, *13*, 489–495. https://doi.org/10.1007/s12182-016-0108-3.
151. Mottahedin, M.; Varaminian, F.; Mafakheri, K. Modeling of methane and ethane hydrate formation kinetics based on non-equilibrium thermodynamics. *J. Non-Equilib. Thermodyn.* **2011**, *36*, 3–22. https://doi.org/10.1515/jnetdy.2011.002.
152. Hashemi, H.; Babaee, S.; Mohammadi, A.H.; Naidoo, P.; Ramjugernath, D. Experimental study and modeling of the kinetics of refrigerant hydrate formation. *J. Chem. Thermodyn.* **2015**, *82*, 47–52. https://doi.org/10.1016/j.jct.2014.10.017.
153. Hashemi, H.; Babaee, S.; Tumba, K.; Mohammadi, A.H.; Naidoo, P.; Ramjugernath, D. Experimental study and modeling of the kinetics of gas hydrate formation for acetylene, ethylene, propane and propylene in the presence and absence of SDS. *Pet. Sci. Technol.* **2019**, *37*, 506–512. https://doi.org/10.1080/10916466.2018.1531024.
154. Talaghat, M.R.; Esmaeilzadeh, F.; Fathikaljahi, J. Experimental and theoretical investigation of simple gas hydrate formation with or without presence of kinetic inhibitors in a flow mini-loop apparatus. *Fluid Phase Equilib.* **2009**, *279*, 28–40. https://doi.org/10.1016/j.fluid.2009.01.017.
155. Talaghat, M.R. Prediction of induction time for natural gas components during gas hydrate formation in the presence of kinetic hydrate inhibitors in a flow mini-loop apparatus. *Can. J. Chem. Eng.* **2013**, *91*, 790–797. https://doi.org/10.1002/cjce.21693.
156. Saberi, A.; Alamdari, A.; Rasoolzadeh, A.; Mohammadi, A.H. Insights into kinetic inhibition effects of MEG, PVP, and L-tyrosine aqueous solutions on natural gas hydrate formation. *Pet. Sci.* **2021**, *18*, 495–508. https://doi.org/10.1007/s12182-020-00515-0.
157. Aghajanloo, M.; Reza Ehsani, M.; Taheri, Z.; Jafari Behbahani, T.; Mohammadi, A.H.; Mohammad Taheri, M. Kinetics of methane + hydrogen sulfide clathrate hydrate formation in the presence/absence of poly N-vinyl pyrrolidone (PVP) and L-tyrosine: Experimental study and modeling of the induction time. *Chem. Eng. Sci.* **2022**, *250*, 117384. https://doi.org/10.1016/j.ces.2021.117384.
158. Karamoddin, M.; Varaminian, F.; Daraee, M. Kinetic study on the process of $CHClF_2$ (R22) hydrate formation in the presence of SDS surfactant based on chemical affinity. *J. Nat. Gas Sci. Eng.* **2014**, *19*, 46–51. https://doi.org/10.1016/j.jngse.2014.04.013.
159. Naeiji, P.; Arjomandi, A.; Varaminian, F. Amino acids as kinetic inhibitors for tetrahydrofuran hydrate formation: Experimental study and kinetic modeling. *J. Nat. Gas Sci. Eng.* **2014**, *21*, 64–70. https://doi.org/10.1016/j.jngse.2014.07.029.
160. Abbasian Rad, S.; Rostami Khodaverdiloo, K.; Karamoddin, M.; Varaminian, F.; Peyvandi, K. Kinetic study of amino acids inhibition potential of Glycine and l-leucine on the ethane hydrate formation. *J. Nat. Gas Sci. Eng.* **2015**, *26*, 819–826. https://doi.org/10.1016/j.jngse.2015.06.053.
161. Rao, Y.; Wang, S.; Yang, Y.; Jia, R.; Zhou, S.; Zhao, S.; Wen, C. Experimental study and chemical affinity model on the inhibition of CO_2 gas hydrate formation. *Chem. Eng. Sci.* **2023**, *281*, 119158. https://doi.org/10.1016/j.ces.2023.119158.
162. Osei, H.; Bavoh, C.B.; Lal, B. Research Advances in Machine Learning Techniques in Gas Hydrate Applications. *ACS Omega* **2024**, *9*, 4210–4228. https://doi.org/10.1021/acsomega.3c04825.
163. Nasir, Q.; Abdul Majeed, W.S.; Suleman, H. Predicting Gas Hydrate Equilibria in Multicomponent Systems with a Machine Learning Approach. *Chem. Eng. Technol.* **2023**, *46*, 1854–1867. https://doi.org/10.1002/ceat.202300055.
164. Elgibaly, A.A.; Elkamel, A.M. A new correlation for predicting hydrate formation conditions for various gas mixtures and inhibitors. *Fluid Phase Equilib.* **1998**, *152*, 23–42. https://doi.org/10.1016/S0378-3812(98)00368-9.
165. Abdolrahimi, S.; Nasernejad, B.; Pazuki, G. Prediction of partition coefficients of alkaloids in ionic liquids based aqueous biphasic systems using hybrid group method of data handling (GMDH) neural network. *J. Mol. Liq.* **2014**, *191*, 79–84. https://doi.org/10.1016/j.molliq.2013.11.033.
166. Ahmadi, M.A.; Ebadi, M.; Shokrollahi, A.; Majidi, S.M.J. Evolving artificial neural network and imperialist competitive algorithm for prediction oil flow rate of the reservoir. *Appl. Soft Comput.* **2013**, *13*, 1085–1098. https://doi.org/10.1016/j.asoc.2012.10.009.
167. Rashid, S.; Fayazi, A.; Harimi, B.; Hamidpour, E.; Younesi, S. Evolving a robust approach for accurate prediction of methane hydrate formation temperature in the presence of salt inhibitor. *J. Nat. Gas Sci. Eng.* **2014**, *18*, 194–204. https://doi.org/10.1016/j.jngse.2014.02.005.
168. Vapnik, V.N. *Statistical Learning Theory*; Wiley: Hoboken, NJ, USA, 1998.
169. Baylar, A.; Hanbay, D.; Batan, M. Application of least square support vector machines in the prediction of aeration performance of plunging overfall jets from weirs. *Expert Syst. Appl.* **2009**, *36*, 8368–8374. https://doi.org/10.1016/j.eswa.2008.10.061.

170. Suykens, J.; Vandewalle, J. Least Squares Support Vector Machine Classifiers. *Neural Process. Lett.* **1999**, *9*, 293–300.
171. Burda, M.; Štěpnička, M. lfl: An R package for linguistic fuzzy logic. *Fuzzy Sets Syst.* **2022**, *431*, 1–38. https://doi.org/10.1016/j.fss.2021.07.007.
172. Jane, J.; Ganesh, E. A review on big data with machine learning and fuzzy logic for better decision making. *Int. J. Sci. Technol. Res.* **2019**, *8*, 1221–1225.
173. Takagi, T.; Sugeno, M. Fuzzy identification of systems and its applications to modeling and control. *IEEE Trans. Syst. Man. Cybern.* **1985**, *SMC-15*, 116–132. https://doi.org/10.1109/TSMC.1985.6313399.
174. Kamali, M.Z.M.; Kumaresan, N.; Ratnavelu, K. Takagi–Sugeno fuzzy modelling of some nonlinear problems using ant colony programming. *Appl. Math. Model.* **2017**, *48*, 635–654. https://doi.org/10.1016/j.apm.2017.04.019.
175. Wescoat, E.; Krugh, M.; Mears, L. Random forest regression for predicting an anomalous condition on a UR10 cobot end-effector from purposeful failure data. *Procedia Manuf.* **2021**, *53*, 644–655. https://doi.org/10.1016/j.promfg.2021.06.064.
176. Ezzeldin, R.; Hatata, A. Application of NARX neural network model for discharge prediction through lateral orifices. *Alex. Eng. J.* **2018**, *57*, 2991–2998. https://doi.org/10.1016/j.aej.2018.04.001.
177. Chapoy, A.; Mohammadi, A.H.; Richon, D. Predicting the Hydrate Stability Zones of Natural Gases Using Artificial Neural Networks. *Oil Gas Sci. Technol.-Rev. Ifp* **2007**, *62*, 701–706. https://doi.org/10.2516/ogst:2007048.
178. Ghiasi, M.M.; Yarveicy, H.; Arabloo, M.; Mohammadi, A.H.; Behbahani, R.M. Modeling of stability conditions of natural gas clathrate hydrates using least squares support vector machine approach. *J. Mol. Liq.* **2016**, *223*, 1081–1092. https://doi.org/10.1016/j.molliq.2016.09.009.
179. Yarveicy, H.; Ghiasi, M.M. Modeling of gas hydrate phase equilibria: Extremely randomized trees and LSSVM approaches. *J. Mol. Liq.* **2017**, *243*, 533–541. https://doi.org/10.1016/j.molliq.2017.08.053.
180. Qin, H.; Srivastava, V.; Wang, H.; Zerpa, L.E.; Koh, C.A. Machine Learning Models to Predict Gas Hydrate Plugging Risks Using Flowloop and Field Data. In Proceedings of the Offshore Technology Conference, Houston, TX, USA, 6–9 May 2019. https://doi.org/10.4043/29411-MS.
181. Acharya, P.V.; Bahadur, V. Thermodynamic features-driven machine learning-based predictions of clathrate hydrate equilibria in the presence of electrolytes. *Fluid Phase Equilib.* **2021**, *530*, 112894. https://doi.org/10.1016/j.fluid.2020.112894.
182. Keshvari, S.; Farizhendi, S.A.; Ghiasi, M.M.; Mohammadi, A.H. AdaBoost Metalearning Methodology for Modeling the Incipient Dissociation Conditions of Clathrate Hydrates. *ACS Omega* **2021**, *6*, 26919–26931. https://doi.org/10.1021/acsomega.1c03214.
183. Xu, H.; Jiao, Z.; Zhang, Z.; Huffman, M.; Wang, Q. Prediction of methane hydrate formation conditions in salt water using machine learning algorithms. *Comput. Chem. Eng.* **2021**, *151*, 107358. https://doi.org/10.1016/j.compchemeng.2021.107358.
184. He, W. Study on Model of Natural Gas Hydrate Formation Based on Extremely Randomized Trees. *J. Phys. Conf. Ser.* **2022**, *2263*, 012022. https://doi.org/10.1088/1742-6596/2263/1/012022.
185. Jalalnezhad, M.J.; Ranjbar, M.; Sarafi, A.; Nezamabadi, P.H. Modeling of Gas hydrate formation in the Presence of Inhibitors by Intelligent systems. *J. Chem. Pet. Eng.* **2015**, *49*, 101–108. Available online: https://www.sid.ir/fileserver/je/136220150201 (accessed on 12 June 2024).
186. Zare, M. Investigation of Methane Hydrate Formation Kinetics Using Machine Learning and Computational Fluid Dynamics Tools. Master's Thesis, Memorial University of Newfoundland, St. John's, NL, Canada, October 2022. https://doi.org/10.48336/3R1B-A585.
187. Klamt, A. Conductor-like Screening Model for Real Solvents: A New Approach to the Quantitative Calculation of Solvation Phenomena. *J. Phys. Chem.* **1995**, *99*, 2224–2235. https://doi.org/10.1021/j100007a062.
188. Klamt, A.; Eckert, F. COSMO-RS: A novel and efficient method for the a priori prediction of thermophysical data of liquids. *Fluid Phase Equilib.* **2000**, *172*, 43–72. https://doi.org/10.1016/S0378-3812(00)00357-5.
189. Ferreira, A.R.; Freire, M.G.; Ribeiro, J.C.; Lopes, F.M.; Crespo, J.G.; Coutinho, J.A.P. Overview of the Liquid–Liquid Equilibria of Ternary Systems Composed of Ionic Liquid and Aromatic and Aliphatic Hydrocarbons, and Their Modeling by COSMO-RS. *Ind. Eng. Chem. Res.* **2012**, *51*, 3483–3507. https://doi.org/10.1021/ie2025322.
190. Lei, Z.; Zhang, B.; Zhu, J.; Gong, W.; Lü, J.; Li, Y. Solubility of CO_2 in Methanol, 1-Octyl-3-methylimidazolium Bis(trifluoromethylsulfonyl)imide, and Their Mixtures. *Chin. J. Chem. Eng.* **2013**, *21*, 310–317. https://doi.org/10.1016/S1004-9541(13)60464-4.
191. Kato, R.; Gmehling, J. Systems with ionic liquids: Measurement of VLE and γ^{∞} data and prediction of their thermodynamic behavior using original UNIFAC, mod. UNIFAC(Do) and COSMO-RS(Ol). *J. Chem. Thermodyn.* **2005**, *37*, 603–619. https://doi.org/10.1016/j.jct.2005.04.010.
192. Gonfa, G.; Bustam, M.A.; Sharif, A.M.; Mohamad, N.; Ullah, S. Tuning ionic liquids for natural gas dehydration using COSMO-RS methodology. *J. Nat. Gas Sci. Eng.* **2015**, *27*, 1141–1148. https://doi.org/10.1016/j.jngse.2015.09.062.
193. Aissaoui, T.; Benguerba, Y.; AlOmar, M.K.; AlNashef, I.M. Computational investigation of the microstructural characteristics and physical properties of glycerol-based deep eutectic solvents. *J. Mol. Model.* **2017**, *23*, 277. https://doi.org/10.1007/s00894-017-3450-5.
194. Benabid, S.; Benguerba, Y.; AlNashef, I.M.; Haddaoui, N. Theoretical study of physicochemical properties of selected ammonium salt-based deep eutectic solvents. *J. Mol. Liq.* **2019**, *285*, 38–46. https://doi.org/10.1016/j.molliq.2019.04.052.
195. Benguerba, Y.; Alnashef, I.M.; Erto, A.; Balsamo, M.; Ernst, B. A quantitative prediction of the viscosity of amine based DESs using Sσ-profile molecular descriptors. *J. Mol. Struct.* **2019**, *1184*, 357–363. https://doi.org/10.1016/j.molstruc.2019.02.052.

196. Claudio, A.F.M.; Swift, L.; Hallett, J.P.; Welton, T.; Coutinho, J.A.P.; Freire, M.G. Extended scale for the hydrogen-bond basicity of ionic liquids. *Phys. Chem. Chem. Phys.* **2014**, *16*, 6593–6601.
197. Abraham, M.H.; Grellier, P.L.; Kamlet, M.J.; Doherty, R.M.; Taft, R.W.; Abboud, J.L.M. The use of scales of hydrogen-bond acidity and basicity in organic chemistry. *Rev. Port. Quím.* **1989**, *31*, 85.
198. Klamt, A. COSMO-RS for aqueous solvation and interfaces. *Fluid Phase Equilib.* **2016**, *407*, 152–158. https://doi.org/10.1016/j.fluid.2015.05.027.
199. Bavoh, C.B.; Lal, B.; Nashed, O.; Khan, M.S.; Keong, L.K.; Bustam, M.A. COSMO-RS: An ionic liquid prescreening tool for gas hydrate mitigation. *Chin. J. Chem. Eng.* **2016**, *24*, 1619–1624. https://doi.org/10.1016/j.cjche.2016.07.014.
200. Khan, M.S.; Liew, C.S.; Kurnia, K.A.; Cornelius, B.; Lal, B. Application of COSMO-RS in Investigating Ionic Liquid as Thermodynamic Hydrate Inhibitor for Methane Hydrate. *Procedia Eng.* **2016**, *148*, 862–869. https://doi.org/10.1016/j.proeng.2016.06.452.
201. Sulaimon, A.A.; Tajuddin, M.Z.M. Application of COSMO-RS for pre-screening ionic liquids as thermodynamic gas hydrate inhibitor. *Fluid Phase Equilib.* **2017**, *450*, 194–199. https://doi.org/10.1016/j.fluid.2017.07.023.
202. Bavoh, C.B.; Partoon, B.; Lal, B.; Gonfa, G.; Foo Khor, S.; Sharif, A.M. Inhibition effect of amino acids on carbon dioxide hydrate. *Chem. Eng. Sci.* **2017**, *171*, 331–339. https://doi.org/10.1016/j.ces.2017.05.046.
203. Khan, M.S.; Partoon, B.; Bavoh, C.B.; Lal, B.; Mellon, N.B. Influence of tetramethylammonium hydroxide on methane and carbon dioxide gas hydrate phase equilibrium conditions. *Fluid Phase Equilib.* **2017**, *440*, 1–8. https://doi.org/10.1016/j.fluid.2017.02.011.
204. Lee, D.; Go, W.; Seo, Y. Synergistic kinetic inhibition of amino acids and ionic liquids on CH_4 hydrate for flow assurance. *Fuel* **2020**, *263*, 116689. https://doi.org/10.1016/j.fuel.2019.116689.
205. Saad Khan, M.; Lal, B. Pre-Screening of Ionic Liquids as Gas Hydrate Inhibitor via Application of COSMO-RS for Methane Hydrate. In *Solvents, Ionic Liquids and Solvent Effects*; IntechOpen: London, UK, 2020. https://doi.org/10.5772/intechopen.86847.
206. Sulaimon, A.A.; Masri, A.N.; Ahmad Shahpin, M.H.; Othman Zailani, N.H.Z.; Baharuddin, S.N.A.; Moniruzzaman, M.; Salleh, I.K.; Saaid, I.M. Synthesis of dihydrogen phosphate-based ionic liquids: Experimental and COSMO-RS based investigation for methane hydrate inhibition. *J. Mol. Liq.* **2020**, *319*, 114092. https://doi.org/10.1016/j.molliq.2020.114092.
207. Lee, D.; Go, W.; Oh, J.; Lee, J.; Jo, I.; Kim, K.-S.; Seo, Y. Thermodynamic inhibition effects of an ionic liquid (choline chloride), a naturally derived substance (urea), and their mixture (deep eutectic solvent) on CH_4 hydrates. *Chem. Eng. J.* **2020**, *399*, 125830. https://doi.org/10.1016/j.cej.2020.125830.
208. Hussain, H.H.; Husin, H. The effect of synergistic amino acids-ionic liquids in methane hydrate inhibition by COSMO-RS application. *J. Mol. Liq.* **2021**, *321*, 114837. https://doi.org/10.1016/j.molliq.2020.114837.
209. Masri, A.N.; Sulaimon, A.A. Amino acid-based ionic liquids as dual kinetic-thermodynamic methane hydrate inhibitor. *J. Mol. Liq.* **2022**, *349*, 118481. https://doi.org/10.1016/j.molliq.2022.118481.
210. Osei, H. Prediction of Ionic Liquids Methane Hydrate Average Depression Temperature via COSMO-RS. *Trends Pet. Eng.* **2024**, *4*, 1–5. https://doi.org/10.53902/TPE.2024.04.000536.
211. Yue, G.; Liu, Y.; Qin, Y.; Tian, Z.; Zhao, X.; Liu, X.; Du, Z.; Zhang, X.; Guo, X. Effect of ionic liquid on CH_4 hydrate formation thermodynamics. *Can. J. Chem. Eng.* **2024**, *102*, 4440–4451. https://doi.org/10.1002/cjce.25313.

Disclaimer/Publisher's Note: The statements, opinions and data contained in all publications are solely those of the individual author(s) and contributor(s) and not of MDPI and/or the editor(s). MDPI and/or the editor(s) disclaim responsibility for any injury to people or property resulting from any ideas, methods, instructions or products referred to in the content.